

**NIST Measurement Services:**

---

**Measurement Assurance Program  
for the Spectral Density of Relative  
Intensity Noise of Optical Fiber  
Sources near 1550 nm**

**NIST  
Special  
Publication  
250-57**

**Gregory E. Obarski  
Jolene D. Splett**

**NIST**

**National Institute of Standards and Technology**  
Technology Administration, U.S. Department of Commerce



Certain commercial entities, equipment, or materials may be identified in this document in order to describe an experimental procedure or concept adequately. Such identification is not intended to imply recommendation or endorsement by the National Institute of Standards and Technology, nor is it intended to imply that the entities, materials, or equipment are necessarily the best available for the purpose.

**National Institute of Standards and Technology Special Publication 250-57**  
**Natl. Inst. Stand. Technol. Spec. Publ. 250-57, 96 pages (September 2000)**  
**CODEN: NSPUE2**

**U.S. GOVERNMENT PRINTING OFFICE**  
**WASHINGTON: 2000**

---

For sale by the Superintendent of Documents, U.S. Government Printing Office, Washington, DC 20402-9325

## Contents

1.	Introduction .....	2
2.	Background .....	4
	2.1 Definition of the RIN of an Optical Source .....	6
	2.2 Application of Laser RIN to Noise Figure of Optical Amplifiers; Electrical Methods ..	7
	2.3 Measurement of RIN .....	9
3.	A RIN Standard Based on Two Different Methods .....	10
	3.1 Form of the RIN Standard or Primary Method .....	10
	3.2 Source RIN of the Secondary Method .....	11
4.	Theory of the Spectral Density of the RIN .....	11
	4.1 Complete Derivation of the Spectral Density of the RIN from the Optical Field Correlations and the Semiclassical Theory of the Photodetection of Light .....	12
	4.2 Numerical Formulation of RIN in the Wavelength Representation .....	18
5.	Accurate Determination of RIN Requires Precise Calibration of Optical Spectrum Analyzer Parameters .....	21
	5.1 Measurement of Resolution Bandwidth and Its Uncertainty .....	21
	5.2 Measurement of Wavelength Error and Distortion .....	22
	5.3 Nonlinearity of the Optical Power Spectral Density Scale .....	23
6.	Some Properties of the RIN Standard .....	24
	6.1 Polarization .....	24
	6.2 Absence of Ripple .....	24
	6.3 RIN of Various Filters of Exact Mathematical Shape; Dependence on Filter Bandwidth and Shape .....	25
	6.4 Measured RIN of Three Different Filters When Linked to the Same EDFA .....	26
	6.5 Use of Connectors and the Effect of Losses .....	27
	6.6 Combined Effects of Attenuation, Pump Current, and Power Spectral Density Levels	27
7.	Total Uncertainty in the RIN Standard .....	30
	7.1 Repeatability Error .....	30
	7.2 Measurement Error From the OSA Parameters .....	31
	7.3 Combined Standard Uncertainty .....	34
8.	Achieving the Poisson Limit .....	35
	8.1 The DFB Laser of the Secondary Method Has Nearly Poisson-Limited RIN .....	36
9.	RIN System Calibration Using the Standard and the Laser .....	37
	9.1 Derivation of the Calibration Equations For the Standard and Secondary Methods ..	38

9.2	Equivalence of the Calibration Functions	39
10.	Two Methods Applied to the NIST RIN System Give Similar Results	40
10.1	Quantitative Comparison of Calibration Results from the Two Methods	40
10.2	Relative Stability of Two Different EDFAs With Respect to the Poisson Laser	45
10.3	Methods Compare Favorably Under Use of Variance Analysis	45
10.4	F-ratio Test Yields Similarity in the Variability of the Calibration Functions	46
11.	Maintaining a Measurement Assurance Program	48
11.1	Maintaining the RIN Standard	48
11.2	Substitution of Components	48
12.	References	50
Appendix A.	Calibration of the Electrical Spectrum Analyzer; Scale Fidelity Correction	53
Appendix B.	Addition of RIN	54
Appendix C.	Information for Applying the RIN Standard	54
Appendix D.	Sample MAP Certificate	55
Appendix E.	Calibration Service	62
Appendix F.	Sample Calibration Certificate	63
Appendix G.	Shipping Instructions	70
Figures		71

# Measurement Assurance Program for the Spectral Density of Relative Intensity Noise of Optical Fiber Sources near 1550 nm

Gregory E. Obarski and Jolene D. Splett

National Institute of Standards and Technology  
325 Broadway  
Boulder, Colorado 80303

This paper provides the documentation to establish a measurement assurance program (MAP) for the spectral density of relative intensity noise (RIN) of optical sources. A standard is made available to industry for high-precision calibration of RIN measurement systems. The device is an erbium-doped fiber amplifier (EDFA) to which is coupled a linear polarizer followed by a narrow pass-band optical filter. Measurements show that the spectral density of the RIN is invariant under attenuation and pump current, and constant from zero to many tens of gigahertz. These properties render it suitable as a standard for the calibration of high-speed systems. We characterize the device for use as a standard in the 1550 nm wavelength range over a radio-frequency (rf) baseband of 0.1 to 1.1 GHz. For the typical device studied in depth, the magnitude of the RIN is  $-109.9$  dB/Hz with uncertainty  $\leq 0.12$  dB over the entire bandwidth. Since the behavior of the RIN standard can be determined from physical theory, we give a thorough derivation of the spectral density of RIN in the frequency representation. This derivation has been absent from the literature. We use this derivation to formulate the needed numerical RIN equations in spatial wavelength coordinates that are used to determine the RIN from optical power spectral density measurements made with a calibrated optical spectrum analyzer. The standard is then applied to calibrate a NIST RIN measurement system. To further validate the standard we develop a second calibration method based on a distributed-feedback (DFB) laser having Poisson-limited RIN. We apply each method to determine the frequency-

dependent calibration function ( $\kappa$ ) of our RIN system and derive the equation that relates them. A comparison of the calibration functions obtained from measurements using the two methods agrees well with the theory developed. The relative uncertainty in their difference is similar to the relative uncertainty in the RIN of the standard. Application of a statistical F-ratio test demonstrates that the variability in  $\kappa$  of the two methods is similar. Thus we establish a RIN standard that compares favorably with a second independent method (Poisson-limited laser) based on rigorous physical theory, high-precision measurements, and thorough statistical analyses.

Key words: calibration; measurement assurance; optical fiber sources; Poisson-limited laser; relative intensity noise; spectral density; transfer standard

## 1. Introduction

Increasing demand for greater bandwidth in optical communications systems has brought to fruition laser transmitters and optical fiber amplifiers with very-low relative intensity noise (RIN) and noise figure, respectively. In this report we present a method for high-precision calibration of RIN measurement systems (where RIN means the spectral density of the relative intensity noise). A standard is made available to industry in the form of an erbium-doped fiber amplifier (EDFA) whose output is coupled to a linear polarizer followed by a narrow-band filter. We characterize a typical device for use as a standard in the 1550 nm wavelength range over an rf frequency baseband of 0.1 GHz to 1.1 GHz. However, the spectral density of the RIN is very nearly constant from zero to many tens of gigahertz, rendering it suitable for calibration of systems of greater bandwidth. Thus, depending on future requirements of industry, we will be able to certify the RIN standard at higher bandwidths by using a higher bandwidth pre-amplifier in the RIN system and applying identical calibration techniques.

The RIN of a typical device studied has a magnitude  $-109.9$  dB/Hz, which can be decreased by using a filter of greater bandwidth. The combined standard uncertainty in the RIN, over the

entire bandwidth, ranges from 0.036 dB/Hz to 0.12 dB/Hz, depending on the filter used. The EDFA's built-in optical isolator, along with the property of invariance of the RIN under attenuation, allows for the convenient use of fiber connectors. We chose a good-quality FC/PC connector, with all components pigtailed to standard single-mode fiber. The invariance under attenuation allows the user to achieve noise power levels on their electrical spectrum analyzer (ESA) to match the values expected when measuring unknown devices.

Accurate specification of the RIN requires that we develop the underlying physical theory from fundamental principles, then apply it to formulate a numerical representation for the RIN. We then developed the metrology to describe the interaction of a potential standard device with a RIN measurement system. This yielded a frequency-dependent calibration function specific to the RIN system under calibration. To validate the device as a standard, we developed a second calibration method based on a distributed-feedback (DFB) laser whose RIN is specified by the manufacturer to be less than  $-172$  dB/Hz. We demonstrated that under sufficient attenuation, the RIN of this source becomes Poisson limited. Using this method to calibrate our RIN system also yielded a similar calibration function ( $\text{Kappa}$ ). By applying the RIN equations for each method to calibrate the RIN system, we derived an exact expression that equates their calibration functions and use it to compare the methods. A typical value for the difference between the functions obtained from each method, as averaged over the 601 frequency points in a span, falls in the range from 0.04 dB to 0.2 dB. Such values are comparable to the relative uncertainty in the RIN of the standard (0.12 dB). Application of a statistical F-ratio test demonstrates that the variability in  $\text{Kappa}$  of the two methods is similar. Thus the RIN standard compares favorably with the Poisson-limited laser. We selected the EDFA method for the standard because it is the most stable, robust, and portable of the two RIN sources. However, in principle either method could be used for the standard, in that either method would produce nearly equivalent results if applied to similar RIN measurement systems.

A calibrated RIN system has two immediate applications that illustrate the need for a measurement assurance program. First, it is needed for precise measurement of the RIN of lasers used in optical communications systems. This demand is of increasing importance as efforts are broadened to create lasers with RIN approaching the standard quantum limit. Second, it is useful

in determining the noise figure of optical amplifiers. In the future we plan to develop a standard (also based on a MAP) specifically for noise figure of optical amplifiers. This latter device will be used to calibrate optical noise figure measurement systems based on electrical spectrum analyzers.

We will attempt to establish the MAP so that future changes can be made to the various components that compose the standard and the measurement apparatus with little or no additional documentation. These might include the EDFA, polarizer, and filter that compose a standard, the optical spectrum analyzer, and RIN system components such as the pre-amplifier, photodetector, bias-tee, electrical spectrum analyzer, and voltmeter.

Herein we refer to the EDFA-based standard as the primary method and the Poisson-limited laser as the secondary method. To distinguish between the use of two different EDFAs and three filters as components of the standard we use the notation EDFA1, EDFA2, and F1, F2, F3, respectively. The bulk of our measurements and analysis was performed on results using EDFA2 with F1. Thus the standard has implicit in its definition the use of EDFA2 and F1. For brevity, instead of denoting the standard by EDFA + P + F, we omit the polarizer, P, and write EDFA + F, keeping in mind that the polarizer is present unless otherwise specified. Finally, a brief discussion of RIN expressed in logarithmic units is given in Appendix B for the reader unfamiliar with this subject.

## **2. Background**

RIN is a concept that is often associated with optical data transmission using diode lasers as the transmitters. However, the basic ideas of RIN are applicable to all classes of lasers as well as almost all optical sources. In analog communications, such as cable television, total RIN within the system bandwidth can limit the signal-to-noise ratio. In high-speed digital systems, RIN can limit the bit-error-rate (BER) and system performance under certain conditions. A laser's high-frequency RIN spectrum often contains a well-defined peak at the relaxation oscillation frequency; for many classes of lasers this peak can be used to deduce the maximum intrinsic modulation frequency for a specific laser. Knowledge of RIN can be applied to the design of new lasers to give improved performance for specific applications. Very low-RIN lasers are used to determine



the noise figure of the optical fiber amplifiers that are essential for building faster and more efficient optical communications systems. The demand for better techniques to calibrate a RIN measurement system's response and sensitivity is also increasing with the appearance of commercial distributed-feedback lasers and diode-pumped Nd:YAG lasers having very low RIN. Typical values of RIN range from  $-110$  dB/Hz to  $-130$  dB/Hz for inexpensive multimode edge emitting diode lasers, and less than  $-170$  dB/Hz for high quality DFB diode lasers.

The RIN of an optical source can arise from a variety of variables and atomic parameters. In this report, we are interested mainly in the RIN of semiconductor lasers and thermal light sources. For semiconductor lasers, the most important parameters are frequency, source output power, temperature, modulation frequency, time delay and magnitude of optical feedback, mode suppression ratio, and relaxation oscillation frequency [1]. For certain kinds of multimode lasers, RIN can be greatly affected by system components which have polarization or wavelength-selective properties [2]. The predominant source of RIN, however, is usually spontaneous emission. Thus the low-frequency RIN of a laser is a maximum just above threshold, diminishing with increasing output power. But it can be greatly increased by optical feedback, even at high output power. For semiconductor lasers such as the DFB laser used for the secondary method of this MAP, the RIN can be formulated by inclusion of Langevin noise sources in the differential rate equations for the photon and carrier densities [3, 4]. Semiconductor laser RIN has important applications in optical communications systems [5]. The source RIN of the standard or primary method, however, will be shown to arise from the amplified spontaneous emission (ASE) of an EDFA. Such fluctuations, which are described by Bose-Einstein statistics, can be approximated by thermal light [6, 7].

Other calibration sources that might apply to calibration of RIN measurement systems are fast-pulse lasers, broadband sources such as light-emitting diodes, and a heterodyne method in which the beat frequency of two tunable lasers is used to determine the frequency response of ultra-high speed photoreceivers. We note that the filtered EDFA method developed herein contains the information for performing such a frequency-response calibration.

## 2.1 Definition of the RIN of an Optical Source

RIN [1, 3, 8] can be precisely calculated from the autocorrelation integral of optical power fluctuations divided by total power squared. These temporal fluctuations can also be expressed in terms of their spectral density via the Fourier transform of the autocorrelation integral. An optical source of output power  $P(t)$  and fluctuation  $\delta P(t)$  has a total RIN,  $RIN_T$ , given by the ratio of the mean square of the fluctuation to the square of the average power,

$$RIN_T = \frac{\langle \delta P(t)^2 \rangle}{\langle P(t) \rangle^2}, \quad (2.1.1)$$

where the time average  $\langle \delta P(t)^2 \rangle$  arises from the autocorrelation function  $\lambda(\tau) = \langle \delta P(t) \delta P(t + \tau) \rangle$  evaluated at time  $\tau = 0$ . The total RIN, which is dimensionless, can be represented in the frequency domain by defining a RIN spectral density, which we simply refer to as the RIN. Then  $RIN_T$  is also the integral of the RIN,  $R(\nu)$ , over all frequencies,

$$RIN_T = \int_0^{\infty} R(\nu) d\nu, \quad (2.1.2)$$

where  $\nu$  is linear optical frequency. This equation holds also for angular frequency units in which  $\omega = 2\pi f$ , since  $\int R(\nu) d\nu = \int R(\omega) d\omega$ . The spectral density of the RIN,  $R(\nu)$ , is derived by application of the Wiener-Khinchine theorem [8] to  $\lambda(\tau)$ . By equating the right hand sides of eqs (2.1.1) and (2.1.2), one can show that this spectral density is

$$R(\nu) = 2 \int_{-\infty}^{\infty} \lambda(\tau) e^{i2\pi\nu\tau} d\tau, \quad (2.1.3)$$

here  $\lambda(\tau) = \langle \Delta I(t)\Delta I(t + \tau) \rangle / \langle I \rangle^2$  is the intensity autocorrelation function ( section 4.1.4). Thus we define the “RIN” of an optical source to be the RIN spectral density,  $R(\nu)$ , and the integral of the RIN to be the “total RIN.”

Our approach is to treat the RIN as consisting of two parts: a Poisson or shot noise component, and a component we call “excess RIN.” The excess RIN propagates unchanged through the system while the Poisson RIN depends on system losses. The “Poisson RIN” is the minimum RIN that can be achieved for classical light. It is often called the standard quantum limit. Classical light obeys an uncertainty relation for which each conjugate field variable is greater than or equal to its minimum value. (The perfectly coherent state is defined as the state when both conjugates are equal and at their minimum.) The excess RIN is non-negative for classical light, whereas it is zero for Poisson light. RIN is specified in units of 1/Hz, or in logarithmic form as decibels per hertz. The total RIN is the sum of the spectral integrals of excess RIN and Poisson RIN [9]; thus, it is dimensionless. To develop a MAP for RIN we characterized two different kinds of sources; a RIN standard (EDFA + F) having nearly excess-limited RIN, and a laser having nearly Poisson-limited RIN.

For light obeying a Poisson distribution, the variance in the photon number is proportional to the photon number. Thus the square of the optical power fluctuations is proportional to the optical power. When represented by a single-sided noise spectrum (positive frequencies only) the Poisson RIN is  $2h\nu/P_0$ , where  $h$  is Planck’s constant,  $\nu$  is photon frequency, and  $P_0$  is optical power. In electrical units it is  $2q/i$ , where  $q$  is electron charge,  $i = \eta q P_0 / h\nu$  is photocurrent, and  $\eta$  is photodetector quantum efficiency. Thus the Poisson RIN in a real detection circuit increases as  $1/\eta$ , so an ideal photodetector ( $\eta = 1$ ) would detect the laser’s true RIN.

## **2.2 Application of Laser RIN to Noise Figure of Optical Amplifiers; Electrical Methods**

Accurate measurement of EDFA noise figure is required for the design and development of optical communications systems that rely on amplification to achieve high bandwidths. There is significant interest in applying optical methods to the measurement of the noise figure because they can be quickly applied to the amplifiers as they emerge from the production line. Optical methods, however, are incapable of measuring multipath interference effects which may arise from

reflections within the amplifier, or between it and the span [10]. Recent reports demonstrate accurate determination of noise figure using electrical methods. Electrical measurement methods are becoming increasingly important because they include multipath interference effects, which, however small, are necessary for the higher-speed analog systems.

There are at least two relevant electrical methods for determining optical amplifier noise figure. The first of these, known as the RIN Subtraction Method [11, 12], requires a laser of low RIN, such as a DFB laser with RIN spectral density  $< -160$  dB/Hz. The RIN is measured with a calibrated RIN system such as the one used in the development of this RIN standard. This method yields the frequency-resolved noise figure referenced to baseband frequencies, “f.” It is of special interest here because the RIN explicitly appears in the noise-figure equation. The RIN of the laser is measured before and after transmission through the amplifier. If  $R_L(f)$  is the RIN of the laser (assuming Poisson-limited RIN) and  $R(f)$  the RIN of the amplified signal, then the noise figure is

$$N_f(f) = (R(f) - R_L(f)) \frac{P_0}{2h\xi} + G^{-1}, \quad (2.2.1)$$

where  $P_0$  is optical power,  $\xi$  is laser frequency,  $h$  is Planck’s constant, and  $G$  is amplifier gain. This method requires that the RIN of the amplifier be greater than the signal source’s RIN and detector’s thermal RIN, and also that the signal source’s RIN be greater than the detector’s thermal RIN.

A second electrical method reports lower RIN uncertainty than the RIN Subtraction Method, and has been shown to agree well with the polarization nulling (optical) method [13, 14]. An attenuator is used to equalize the power levels on a photodetector with and without the amplifier present. This results in equal amounts of shot, thermal, and excess RIN levels, all of which vanish from the noise figure equation upon subtraction of the signals. The net result is a simplified determination of the noise figure. Both methods are of paramount importance because each includes contributions to the noise figure of multiple path interference.

### 2.3 Measurement of RIN

We measure RIN in the electrical domain by direct detection, although it can be determined using optical correlation techniques. A general RIN measurement system with losses is shown in Figure 2.3.1. The beam passes through a loss medium, such as an attenuator, and is collected by the photodetector. The RIN,  $R(\nu)$ , is to be determined at reference plane A, before any losses. The Poisson component of the RIN is increased at plane B due to losses, and again at plane C due to inefficiency in the photodetection process. System efficiency can be combined into one factor  $\eta_T = \eta(1 - L)$ , where  $L$  is the fractional loss before the detector. The excess RIN, however, propagates unchanged through the system. If  $R_C(\nu)$  is the measured RIN at plane C (which includes Poisson RIN), then the laser RIN is

$$R_A(\nu) = R_C(\nu) - \frac{2q}{i}(1 - \eta_T) . \quad (2.3.1)$$

The excess RIN,  $R_{ex}(\nu)$ , is determined by subtracting the measured Poisson or shot-noise RIN,  $2q/i$ , from  $R_C(\nu)$ , giving

$$R_{ex}(\nu) = R_C(\nu) - \frac{2q}{i} . \quad (2.3.2)$$

This last equation is equivalent to subtracting the Poisson RIN from the RIN at plane A,

$$R_{ex}(\nu) = R_A(\nu) - \frac{2h\xi}{P_0} , \quad (2.3.3)$$

where  $\xi$  and  $P_0$  are the laser frequency and power (at plane A), respectively.

To measure RIN in the electrical domain, a bias tee sends the dc photocurrent produced in a photodetector by a test laser to an ammeter, while the ac noise is amplified and then displayed on a radio-frequency (rf) spectrum analyzer. In the electrical domain we weight the noise power per

unit bandwidth,  $\delta P_e(f)$ , measured on an rf spectrum analyzer, with a linear frequency-dependent calibration function  $\kappa(f)$  for the detection system, and divide by electrical dc power  $P_e$ . We note that  $\kappa(f)$  is proportional to the frequency response of the system, and contains the noise added by the amplifier. If the excess RIN is much greater than the Poisson RIN, or if we avoid system losses, the RIN is

$$R(f) = \frac{\kappa(f) \delta P_e(f)}{P_e}, \quad (2.3.4)$$

where  $\delta P_e(f)$  is the noise after subtracting the thermal noise floor of the ESA.  $\kappa(f)$ , can be obtained from a broadband, flat source of known RIN.

In the electrical domain, the total RIN is also the integral of the RIN over all frequencies, or over the system bandwidth, BW,

$$RIN_T = \int_0^{BW} R(f) df, \quad (2.3.5)$$

Total RIN can be measured with an electrical filter and an rf power meter in place of the spectrum analyzer.

### 3. A RIN Standard Based on Two Different Methods

#### 3.1 Form of the RIN Standard or Primary Method

The form of the RIN standard is shown in Figure 3.1.1. The ASE from an erbium-doped fiber amplifier (EDFA) is fed through a linear polarizer followed by a narrow band optical filter (1 nm to 3 nm) centered in the 1550 nm range [15,16]. The wavelength spectrum of the ASE from one of the amplifiers used in this study, EDFA1, is shown in Figure 3.1.2. The EDFA has a built-in optical isolator and was chosen for its ruggedness. To simplify operation for the customer, we arranged for a simplified front panel display with only an on/off power switch. The linear polarizer eliminates the potential for a polarization imbalance between orthogonally polarized modes which

might occur due to fiber bending. The excess RIN of this device is much greater than its Poisson RIN, so that the total RIN can be considered excess RIN. The shape and bandwidth of the filter determine the RIN.

Figure 3.1.3 shows the setup for measurement of the standard's power spectral density (OPSD) using a diffraction grating-type optical spectrum analyzer. For a single measurement, the OSA is set to average four sweeps on high sensitivity with the resolution bandwidth set at the minimum of 0.05 nm. High-quality FC/PC connectors and single-mode fiber are used. Points 1, 2, 3, and 4 represent locations where connectors were routinely disconnected to change components. We later show that this procedure can change the power loss through the fiber transmission line, but has no significant effect on the RIN which is invariant under attenuation. Also, we will show that the EDFA's optical isolator sufficiently shields it from backreflections due to the connector's small but finite return loss, and prevents ripple on the output signal of the RIN standard.

### **3.2 Source RIN of the Secondary Method**

To establish a MAP, a secondary method was used to calibrate our RIN measurement system. Results were compared with those obtained from the standard (or primary method). The secondary method was a DFB laser having very low excess RIN, specified by the manufacturer to be  $\leq -172$  dB/Hz at the recommended operating power of 28 mW. In section 6.6 we will show that attenuation of the light to a fraction of a milliwatt results in practically Poisson-limited RIN. This result follows because under attenuation the excess RIN is invariant but the Poisson RIN increases. Thus, the RIN of the standard is described by the excess RIN of filtered ASE, and the RIN of the laser is described by Poisson RIN.

## **4. Theory of the Spectral Density of the RIN**

The spectral density of the RIN of the standard used in this MAP, as approximated by thermal light, must be derived from physical theory, as the RIN cannot be directly verified through experimental means. In practice, our theory must yield the RIN from knowledge of the OPSD as

measured by an optical spectrum analyzer (OSA). Much of the fundamental theory is greatly developed by Mandel and Wolf [17]. However, it is sketchy in places, and not formulated in terms of RIN explicitly. It also contains an acknowledged error of a factor of two in one of the key results [18]. Thus we need to give a complete and accurate derivation of the RIN spectrum in the frequency and spatial wavelength representations. Although the amplitude fluctuations can be described by distributions of photon number density with respect to time, this method need not be applied to the filtered ASE of the EDFA (RIN standard) or the Poisson light of the laser. To develop a useful formalism we applied the theory of fluctuations to the conversion of optical noise on the source to electronic noise within the RIN measurement system. The correlation between the amplitude fluctuations of partially or totally coherent light and those of the associated photocurrent are well known [17]. In formulating the RIN in terms of the spatial representation, we note that a fluctuation of the intensity in time gives rise to a frequency component. Such Fourier frequency components manifest themselves as a spatial wavelength distribution in the grating-type optical spectrum analyzer used to measure the power spectral density. Thus we seek to represent the temporal Fourier transform of the amplitude noise as fluctuations in either frequency or wavelength. Any contribution from the Poisson or standard quantum limit will be considered negligible compared to the filtered ASE of the EDFA. Since our derivation follows that of Mandel and Wolf, we use their notation to minimize any confusion that may arise.

#### **4.1 Complete Derivation of the Spectral Density of the RIN From the Optical Field Correlations and the Semiclassical Theory of the Photodetection of Light**

From the general form for the autocorrelation of the photocurrent fluctuations ([17], section 8.4.1, eq (9.8.10)), we derive the spectral density of the current fluctuations in terms of measurable quantities ([17], eq (9.8.24)) which is omitted from the text. We then apply the properties of the degree of coherence of the light field ([17], section 8.4.1) to express the RIN as an autocorrelation of a power spectral density function. For completeness we give the results for both polarized and unpolarized light, although we use only polarized light for the standard. Unless specified, all integrals in both the time and frequency representations are double-sided; thus their limits run from minus to plus infinity.



To relate the fluctuations in photoelectric current  $\Delta j(t)$  that arise from the intensity fluctuations of the light field  $\Delta I(t)$ , we define the following quantities:  $j(t)$  is the total photoelectric current in the photodetector circuit at time  $t$ ,  $k$  the distribution of current pulses, and  $\eta$  the quantum efficiency of the detection system. Then the autocorrelation of the current  $\langle \Delta j(t) \Delta j(t + \tau) \rangle$  at delay or correlation time  $\tau$  is related to the autocorrelation of the intensity fluctuations by

$$\begin{aligned} \langle \Delta j(t) \Delta j(t + \tau) \rangle &= \eta \langle I \rangle \int_{-\infty}^{\infty} k(t') k(t' + \tau) dt' \\ &+ \eta^2 \int_{-\infty}^{\infty} \int_{-\infty}^{\infty} k(t') k(t'') \langle \Delta I(t) \Delta I(t + t' - t'' + \tau) \rangle dt' dt'' , \end{aligned} \quad (4.1.1)$$

where  $t'$  and  $t''$  are just dummy integration variables and the first term represents the shot noise of the photocurrent ([17], eq (9.8.10)). To later arrive at a functional form for the RIN, we define some quantities connecting the time and frequency domains. Recall that the spectral density of the current fluctuations  $\chi(\omega)$  is the Fourier transform of the photocurrent autocorrelation function,

$$\chi(\omega) = \int_{-\infty}^{\infty} \langle \Delta j(t) \Delta j(t + \tau) \rangle e^{i\omega\tau} d\tau . \quad (4.1.2)$$

To represent the frequency response of the RIN system, we define the Fourier transform of  $k(t)$  as  $K(\omega)$ :

$$K(\omega) = \int_{-\infty}^{\infty} k(t) e^{i\omega t} dt . \quad (4.1.3)$$

To represent the intensity fluctuations in the time domain, we define  $\lambda(\tau)$  as the autocorrelation in time of the light intensity fluctuations divided by the square of the average intensity:

$$\lambda(\tau) = \frac{\langle \Delta I(t) \Delta I(t+\tau) \rangle}{\langle I \rangle^2} . \quad (4.1.4)$$

Then the Fourier transform of  $\lambda(\tau)$  is the spectral density, which we denote by  $\psi(\omega)$ . For unpolarized thermal light

$$\psi(\omega) = \int_{-\infty}^{\infty} \lambda(\tau) e^{i\omega\tau} d\tau , \quad (4.1.5)$$

which is proportional to the RIN.

We now proceed to derive eq (9.8.24) of Mandel and Wolf [17]. Substituting the above relations into eq (4.1.2) above yields for  $\chi(\omega)$ ,

$$\begin{aligned} \chi(\omega) &= \int_{-\infty}^{\infty} e^{i\omega\tau} d\tau \left[ \eta \langle I \rangle \int_{-\infty}^{\infty} k(t') k(t'+\tau) dt' \right. \\ &\quad \left. + \eta^2 \int_{-\infty}^{\infty} \int_{-\infty}^{\infty} k(t') k(t'') \langle \Delta I(t) \Delta I(t+t'-t''+\tau) \rangle dt' dt'' \right] \\ &= \eta \langle I \rangle |K(\omega)|^2 \\ &\quad + \eta^2 \langle I \rangle^2 \int_{-\infty}^{\infty} \left[ \int_{-\infty}^{\infty} \int_{-\infty}^{\infty} \frac{k(t') k(t'') \langle \Delta I(t) \Delta I(t+t'-t''+\tau) \rangle}{\langle I \rangle^2} dt' dt'' \right] e^{i\omega\tau} d\tau \\ &= \eta \langle I \rangle |K(\omega)|^2 + U(\omega). \end{aligned} \quad (4.1.6)$$

If we define a function  $G(\tau)$  as

$$G(\tau) = \int_{-\infty}^{\infty} \int_{-\infty}^{\infty} \frac{k(t'')k(t')\langle\Delta I(t)\Delta I(t+t'-t''+\tau)\rangle}{\langle I \rangle^2} dt' dt'', \quad (4.1.7)$$

then we observe that  $U(\omega)$  is the Fourier Transform of  $G(\tau)$ ,

$$\begin{aligned} U(\omega) &= \eta^2 \langle I \rangle^2 \int_{-\infty}^{\infty} G(\tau) e^{i\omega\tau} d\tau \\ &= \eta^2 \langle I \rangle^2 \mathcal{F}\{G(\tau)\} \\ &= \eta^2 \langle I \rangle^2 \int_{-\infty}^{\infty} \left[ \int_{-\infty}^{\infty} \int_{-\infty}^{\infty} \frac{k(t'')k(t')\langle\Delta I(t)\Delta I(t+t'-t''+\tau)\rangle}{\langle I \rangle^2} dt' dt'' \right] e^{i\omega\tau} d\tau. \end{aligned} \quad (4.1.8)$$

Since  $G$  is a function only of  $\tau$ , we can apply the shifting property of Fourier transforms to the dummy variables  $t'$ , and  $t''$  in  $\Delta I(t+t'-t''+\tau)$  before integrating. If  $\mathcal{F}$  represents the Fourier Transform, then the result is

$$\mathcal{F}\{\Delta I(t+t'-t''+\tau)\} = \mathcal{F}\{\Delta I(t+\tau)\} \cdot e^{-i\omega(t'-t'')} \quad (4.1.9)$$

so that

$$\begin{aligned} U(\omega) &= \eta^2 \langle I \rangle^2 \int_{-\infty}^{\infty} \int_{-\infty}^{\infty} \int_{-\infty}^{\infty} \frac{k(t'')k(t')\langle\Delta I(t)\Delta I(t+\tau)\rangle}{\langle I \rangle^2} e^{i\omega(t'-t''+\tau)} dt' dt'' d\tau \\ &= \eta^2 \langle I \rangle^2 \int_{-\infty}^{\infty} k(t') e^{i\omega t'} dt' \int_{-\infty}^{\infty} k(t'') e^{-i\omega t''} dt'' \int_{-\infty}^{\infty} \frac{\langle\Delta I(t)\Delta I(t+\tau)\rangle}{\langle I \rangle^2} e^{i\omega\tau} d\tau, \end{aligned} \quad (4.1.10)$$

$$\begin{aligned}
U(\omega) &= \eta^2 \langle I \rangle^2 K(\omega) K(\omega)^* \Psi(\omega) \\
&= \eta^2 \langle I \rangle^2 |K(\omega)|^2 \Psi(\omega).
\end{aligned}
\tag{4.1.11}$$

With these substitutions,  $\chi(\omega)$  becomes

$$\chi(\omega) = \eta \langle I \rangle |K(\omega)|^2 (1 + \eta \langle I \rangle \Psi(\omega)) .
\tag{4.1.12}$$

Thus the spectral density of the electric current fluctuations arises directly from  $\Psi(\omega)$ , which is proportional to the RIN spectral density of the light. For applications regarding this MAP,  $K(\omega)$  is referenced to the baseband frequency, and is proportional to the calibration function to be obtained for the RIN measurement system by application of the standard.

All equations up to this point hold for any kind of light. However, the amplified spontaneous emission of the RIN standard is represented well by treating it as thermal light. As such it is governed by Gaussian statistics, for which all space-time correlation functions of the field can be represented by ones of lower-order ([17], section 8.4.1; see also 1.6.3 and 8.5.3 on Gaussian moment theorem). An important result is that the second-order complex degree of coherence  $\gamma(\tau)$ , from which  $\lambda(\tau)$  is derived, can be found from the first-order space-time correlation function. Thus the normalized intensity correlations for unpolarized thermal light at a single point in space ([17], eqs (8.4.10) and (8.4.24)) can be derived from the degree of coherence:

$$\langle \Delta I(t) \Delta I(t+\tau) \rangle = \frac{\langle I \rangle^2}{2} |\gamma(\tau)|^2 .
\tag{4.1.13}$$

Whereas for polarized thermal light,

$$\langle \Delta I(t) \Delta I(t+\tau) \rangle = \langle I \rangle^2 |\gamma(\tau)|^2 . \quad (4.1.14)$$

Returning to unpolarized thermal light, the autocorrelation of the intensity fluctuations in the time domain is

$$\lambda(\tau) \equiv \frac{\langle \Delta I(t) \Delta I(t+\tau) \rangle}{\langle I \rangle^2} = \frac{|\gamma(\tau)|^2}{2} . \quad (4.1.15)$$

Now the autocorrelation function of a stationary random process and the spectral density of the process form a Fourier-transform pair (Wiener-Khintchine theorem). Thus there exists a Fourier transform of  $\gamma(\tau)$  in the frequency domain that is the normalized spectral density of the optical field [19],

$$\phi(\nu) = \int_{-\infty}^{\infty} \gamma(\tau) e^{-2\pi i \nu \tau} d\tau . \quad (4.1.16)$$

Since  $\phi(\nu)$  is single-sided, the inverse relation is

$$\gamma(\tau) = \int_0^{\infty} \phi(\nu) e^{2\pi i \nu \tau} d\nu . \quad (4.1.17)$$

From eqs (2.1.3) and (4.1.15), the RIN is

$$R(\nu) = \int_{-\infty}^{\infty} |\gamma(\tau)|^2 e^{2\pi i \nu \tau} d\tau = \int_0^{\infty} \phi(\mu) \phi(\mu+\nu) d\mu . \quad (4.1.18)$$

If  $S(\nu)$  is the power spectral density as measured by the OSA, and  $P$  is the total power in the spectrum, then  $\phi(\nu) = S(\nu)/P$ , and the RIN for unpolarized thermal light is

$$R(f) = \int_0^{\infty} \frac{S(\nu)S(\nu+f)d\nu}{P^2} . \quad (4.1.19)$$

For polarized thermal light we need only introduce the same factor of two as appears in eq (4.1.14) for the autocorrelation of the intensity fluctuations,

$$R(f) = 2 \int_0^{\infty} \frac{S(\nu)S(\nu+f)d\nu}{P^2} . \quad (4.1.20)$$

This derivation establishes the RIN equation of the standard from physical theory. The magnitude and uncertainty of the RIN will be determined from measurement of the optical power spectral density of the RIN standard with a well-calibrated OSA. The calibration properties of the RIN measurement system, which to some extent are arbitrary, will be determined from measurement and theory by application of the standard and the secondary method (Poisson-limited laser). The results of the two methods will be compared to verify the equivalence of their calibration properties. The theory of the Poisson laser is historically known and proven by key experiments that relate classical and non-classical states of light.

## 4.2 Numerical Formulation of the RIN in the Wavelength Representation

Having formulated a precise theory for the RIN of the standard, we now develop a numerical representation that accurately treats the experimental data. This can be done in either the frequency or the wavelength representation. As the data are recorded with a grating-type OSA, we seek approximate numerical expressions that will yield the OPSD and the RIN from a finite basis of data points in the wavelength representation specified by the OSA. In the previous section, we showed that the RIN in the frequency representation is the autocorrelation of OPSD

divided by the power squared. If  $\delta p_j(\lambda_j)$  is the optical power measured at wavelength  $\lambda_j$  where resolution bandwidth is  $B_j(\lambda_j)$ , then the optical power spectral density  $S_j(\lambda_j)$  at  $\lambda_j$  is

$$S_j(\lambda_j) = \frac{\delta P_j(\lambda_j)}{B_j(\lambda_j)} . \quad (4.2.1)$$

Then in the wavelength representation

$$RIN(\Lambda) \approx \frac{2}{P^2} \int_0^Z S(\lambda)S(\lambda + \Lambda) d\lambda , \quad (4.2.2)$$

where  $P$  is total optical power,  $\lambda$  is wavelength,  $Z$  is measurement span, and  $\Lambda$  is the shifting parameter in units of wavelength. The integral is not exact since  $\lambda$  and  $\nu$  are inversely proportional ( $\lambda\nu = c$ , from which it follows that  $\Delta\lambda/\Delta\nu = -\lambda^2/c$ ). Thus a 1 Hz bandwidth will give a bandwidth in wavelength units of  $\Delta\lambda = \lambda^2/c$ . This can result in a considerable error in the RIN when the optical power is significant over  $\approx 5$  nm or more of the wavelength span. Thus we first convert from wavelength to frequency units before calculating the RIN.

The total power is obtained from the sum over the incremental power elements in each resolution bandwidth. The OSA used in these developments measures total power according to the relation

$$P = \sum_j \frac{\delta P_j(\lambda_j)}{B_j(\lambda_j)} \cdot \Delta\lambda_j , \quad (4.2.3)$$

where  $\Delta\lambda$  is the wavelength interval defined by dividing the span by the number of data points minus one. Rewriting both the autocorrelation of the power spectral density and the optical power as sums, the RIN evaluated at some arbitrary shift  $\Lambda_i$  is

$$RIN(\Lambda_i) = \frac{2 \sum_j \frac{\delta P_j(\lambda_j)}{B_j(\lambda_j)} \cdot \frac{\delta P_{i+j}(\lambda_{i+j})}{B_{i+j}(\lambda_{i+j})} \cdot \Delta \lambda_j}{\left( \sum_j \frac{\delta P_j(\lambda_j)}{B_j(\lambda_j)} \cdot \Delta \lambda_j \right)^2} \quad (4.2.4)$$

This is the most general expression, and accounts for errors in the RIN due to variation in the wavelength scale (absolute wavelength and wavelength distortion) and resolution bandwidth, as determined over the entire wavelength span. The shifting parameter does not appear explicitly, but is defined to exist at the arbitrary shifting value of  $\Lambda_i = \lambda_i$ . Because the RIN of the standard is very nearly constant from zero shift to many tens of gigahertz, we can simplify this expression by setting  $\Lambda_i = 0$ , which implies  $i = 0$ . This gives

$$RIN(\Lambda=0) = \frac{2 \sum_j \left( \frac{\delta P_j(\lambda_j)}{B_j(\lambda_j)} \right)^2}{\Delta \lambda \left( \sum_j \frac{\delta P_j(\lambda_j)}{B_j(\lambda_j)} \right)^2}, \quad (4.2.5)$$

which is the most general form for the RIN with zero shifting.

Next we consider the shifting equation for the RIN (eq (4.2.4)) when the wavelength distortion is negligible and the resolution bandwidth is constant. Under these conditions,  $\Delta \lambda_j = \Delta \lambda$  and  $B_j(\lambda_j) = B_{i+j}(\lambda_{i+j}) = B$  for all  $i$  and  $j$ . Thus the resolution bandwidth is of no consequence while a  $\Delta \lambda$  remains in the denominator. The RIN becomes

$$RIN_i = \frac{2 \sum_j \delta P_j(\lambda_j) \cdot \delta P_{i+j}(\lambda_{i+j})}{\left( \sum_j \delta P_j(\lambda_j) \right)^2 \cdot \Delta \lambda} \quad (4.2.6)$$



At zero shifting this simplifies to

$$RIN = \frac{2 \sum_j \delta P_j(\lambda_j)^2}{\Delta\lambda \left( \sum_j \delta P_j(\lambda_j) \right)^2} \quad (4.2.7)$$

In section 7, we apply the propagation-of-errors formula to these equations to estimate the total uncertainty in the RIN.

## 5. Accurate Determination of RIN Requires Precise Calibration of Optical Spectrum Analyzer Parameters

Since the RIN of the optically filtered EDFA noise is proportional to the autocorrelation of the optical power spectral density, the optical spectrum must be precisely measured by a well-calibrated OSA. From the numerical equations for the RIN, the OSA parameters to be evaluated for uncertainty are resolution bandwidth, wavelength, and power spectral density. The power spectral density is not a true function because the resolution bandwidth can never be zero. This condition is acceptable since we can account for all errors in the measurement parameters at each point numerically. We convert from wavelength to frequency units since we need to reference the RIN spectrum to the rf-baseband frequency.

### 5.1 Measurement of Resolution Bandwidth and Its Uncertainty

We determined resolution bandwidth over a wide wavelength range by two distinct methods using several narrow-linewidth lasers (linewidth  $\ll$  instrument resolution bandwidth). Among these were a tunable laser (linewidth  $< 1$  MHz) in the 1540 nm to 1580 nm range with wavelength established by a high-accuracy wavemeter (1 ppm), a 1523 nm HeNe laser (linewidth  $< 50$  MHz, and previously developed as a secondary wavelength standard), and a 1310 nm YAG laser for good measure. In the first method, the response of the OSA to the narrow linewidth laser (or delta function input) is read directly from the OSA. The single-wavelength input is broadened by the monochromator, and the resolution bandwidth is equated to the 3 dB bandwidth as read

directly from the OSA. We refer to the broadened curve as the slit function. Figure 5.1.1 shows that the slit function for our OSA is fairly smooth from the peak value down to about 25 dB below peak value, below which it becomes quite irregular. The 1 nm span is centered at 1551 nm, the resolution bandwidth is set at 0.05 nm, and the tunable laser is set at 3 mW optical power. In the second method, the noise-equivalent bandwidth (denoted herein by  $\beta$ ) is calculated and used as the definition of resolution bandwidth. If  $\lambda_0$  is the center wavelength of an arbitrary-shaped slit function  $T(\lambda)$  of peak value  $T(\lambda_0)$ , then

$$\beta = \frac{1}{T(\lambda_0)} \int T(\lambda) d\lambda , \quad (5.1.1)$$

where integration is performed over the entire slit function with the background noise subtracted out. For a perfectly rectangular slit, either method gives the exact answer, while for a distorted slit,  $\beta$  is more accurate because it accounts for the exact slit geometry.

For each method, the tunable laser was set at predetermined wavelengths and the slit function displayed on the OSA. The two methods agree as shown in Figure 5.1.2. For either method, the resolution bandwidth is practically constant over the wavelength range shown. For the 3 dB method, the average resolution bandwidth is 0.041 nm, with standard deviation of 0.001 nm. For the noise equivalent bandwidth, the average is 0.045 nm, with the same standard deviation. We use the latter result because our slit function is irregular. Note that the measured values for the resolution bandwidth are actually smaller than the OSA setting.

## 5.2 Measurement of Wavelength Error and Distortion

The OSA wavelength scale (horizontal axis) undergoes distortion that manifests itself as a nonuniform distribution of data points. The absolute error and distortion in the wavelength scale was determined by comparing the wavelength from a narrow linewidth tunable laser as read by the OSA with the known wavelength as read by a precision wavemeter. OSA data were averaged over four sweeps. For example, a wavelength setting of the tunable laser at 1560 nm yielded a

value of 1559.975 nm when read by the wavemeter. The corresponding OSA wavelength reading was 1559.94 nm. This gives an uncertainty of 0.035 nm (fractional uncertainty of  $22 \cdot 10^{-6}$ ), which falls well within the manufacturer's specifications for wavelength ( $\pm 0.5$  nm over the 350 nm to 1750 nm range). Wavelength error was measured for many points around both 1548 nm to 1560 nm. For the 21 points shown in Figures 5.2.1 and 5.2.2, the standard deviation is 0.042 nm. This agrees with calibration results obtained by the manufacturer at specific wavelengths. For example, application of a HeNe laser of wavelength at 1523.1 nm (in air) yielded a wavelength reading of 1523.13 nm on the OSA. This is an error of 0.03 nm, and in agreement with our average uncertainty of 0.042 nm. Although the error appears to be small, application of the propagation-of-errors formula will later show that it contributes significantly to the total uncertainty in the RIN (section 7.2).

### 5.3 Nonlinearity of the Optical Power Spectral Density Scale

Since the thermal RIN is a ratio of powers squared (eq 4.2.4), and as such is invariant under attenuation, absolute power measurements are not required. This simplifies calibration of the OSA specifically for thermal RIN measurements. However, the potential effect on the numerical RIN of a nonlinear power spectral density across the wavelength span of the OSA must be considered. Also, if a slight attenuation effect existed because of wavelength dispersion from some optical component or connector in the fiber transmission line of the standard, it would couple with the nonlinearity of the spectral responsivity of the OSA. Thus we determine the effect on the RIN of spectral responsivity and attenuation in aggregate, and do not attempt to separate potential contributions that may arise from the two variables. In the simplified eq (4.2.7) for the RIN, a constant linear scaling error, say  $\epsilon$ , would cancel if uniformly applied at every noise power,  $\delta P_j(\lambda_j)$ , over the entire wavelength span. This follows by substituting  $\epsilon \delta P_j(\lambda_j)$  for each term. In general, we expect  $\psi$  to arise mainly from the nonlinear spectral responsivity of the OSA's photodetector and any wavelength dispersing components. As such, it is a measure of the total wavelength or frequency response of the OSA. Thus, on some level of fineness, we expect  $\epsilon_j = \epsilon_j(\lambda_j)$ , so that the uncertainty in noise power will not cancel. In section 6.6, we determine that  $\psi_j$  is a small quantity and devise a measurement scheme in which it need not be determined

explicitly. The error due to noise power measurement will be determined by attenuating the input RIN signal from the standard to fall at predetermined levels on the OSA screen. In addition, RIN measurements under varying conditions of attenuation and EDFA pump current adjusted to yield equal values of power density on the screen will also determine that the nonlinearity in the spectral responsivity is small. Measurements will show that the combined effect is indeed small.

## **6. Some Properties of the RIN Standard**

### **6.1 Polarization**

In section 4.1, we showed that the RIN of the standard was a factor of 2 greater for linearly polarized than for unpolarized thermal light. Thus for unpolarized light fiber bending could imbalance the power transmitted between orthogonally polarized modes and change the RIN by a finite amount. We attempted to measure this effect by changing the curvature of the fiber that links the various components, but found it to be nearly negligible. Nonetheless, we add the polarizer to eliminate potential effects which might arise under varying conditions.

We tested the theoretical relationships derived for the RIN for unpolarized and polarized light. A linearly polarizing isolator determined the polarization behavior of the RIN standard. Measurement of the RIN with and without the polarizing isolator gave a difference of 3.003 dB in the noise power measured on the electrical spectrum analyzer (ESA). This compares well with the 3.0103 dB difference predicted by theory. We note that the RIN system need not be calibrated to perform this measurement because the calibration function cancels in the equations that define the difference in the RIN of the two states; it is only necessary that the measurement be performed at the same ESA settings.

### **6.2 Absence of Ripple**

Low-amplitude ripple for frequencies in the tens of megahertz region was previously observed in EDFAs and attributed to multiple path interference [20]. To test for ripple on the RIN standard we visually inspected the RIN spectrum on the ESA at different frequency spans. Figure 6.2.1 shows the amplitude noise over the total frequency range of interest, 0.1 GHz to 1.1 GHz, with no apparent ripple. Data points are spaced about 1.67 MHz apart. Resolution and

video bandwidths are 300 kHz and 300 Hz, respectively. Figure 6.2.2 shows the frequency band from 700 MHz to 850 MHz devoid of ripple. Data are spread over 0.25 MHz and video bandwidth has been reduced to 100 Hz. Finally, Figure 6.2.3 shows a ripple-free noise spectrum from 500 MHz to 600 MHz. Data points are spaced every 0.166 MHz, and video bandwidth is 30 Hz. Sampling other frequency intervals, such as 100 MHz to 250 MHz, and 400 MHz to 550 MHz (neither shown), also yielded no apparent ripple.

To insure that the RIN standard is indeed free of ripple, we compared the calibration function obtained by applying it to the RIN system with that obtained from a ripple-free independent source (the Poisson laser of method two, see sections 9.1, 9.2, and 10.1). The calibration functions from the two RIN sources are nearly identical, demonstrating that the RIN standard is ripple-free. The absence of a ripple effect indicates that the built-in optical isolator effectively shields the EDFA from feedback.

### **6.3 RIN of Various Filters of Exact Mathematical Shape; Dependence on Filter Bandwidth and Shape**

To understand the behavior and properties of the RIN standard, we can solve the exact RIN equation for filters whose transmittance curves have exact mathematical shapes. Column 2 of Table 1 shows the results for a Gaussian, a Lorentzian, and a rectangular-shaped transmittance filter, with  $\Delta$  the triangle function, the  $C$ 's constants,  $f$  the baseband frequency, and  $B$  the filter bandwidth. In all three cases, the RIN is proportional to the product of the the inverse of the filter bandwidth and a bandwidth-dependent function [16]. It is practically constant to tens or even hundreds of gigahertz, as expected for frequencies that are small compared to the optical bandwidth as shown. From the form of the underlying functions, the magnitude of the RIN can be increased significantly by decreasing the bandwidth.

Table 1. RIN of optical filters whose transmittance curves have exact mathematical shapes.

Spectral density shape	RIN $\equiv R$	Lim $\{\delta R/R\}$ as $f \Rightarrow 0$
Rectangle	$(1/B) \wedge (f/B)$	$\delta B/B$
Gaussian	$(C_1/B) \exp\{-C_2 (f/B)^2\}$	$\delta B/B$
Lorentzian	$(1/B) \{ 1 + (f/B)^2 \}$	$\delta B/B$

In the third column, we list the calculated limit of the variation in the RIN divided by the RIN as the frequency tends toward zero. For all three cases, the result equals the variation in the bandwidth divided by bandwidth. Thus a uniform frequency increment, such as provided by an OSA with a constant-resolution bandwidth, should yield a very precise RIN. RIN calculations give similar results for intermediate shaped filters. However, the RIN of a filter with an asymmetric-transmittance shape may behave differently.

#### 6.4 Measured RIN of Three Different Filters When Linked to the Same EDFA

Figure 6.4.1 shows the optical power spectral density from the OSA for the three filters F1, F2, and F3 used with EDFA2 (each combination a potential RIN standard). Very similar results are also obtained using EDFA1. Filter F1 is quite rectangular in shape and has 3 dB bandwidth of 1.37 nm. Filter F2 is somewhat rectangular, but spreads more quickly toward the wings; it has bandwidth 3.42 nm. Although filter F3 spreads very quickly toward the wings, it has a 3 dB bandwidth of 1.32 nm. Figure 6.4.2 shows that the RIN obtained using all three filters is constant out to tens of gigahertz. The rectangular shaped filter F1 falls off the fastest, since the RIN is an autocorrelation function. Increasing the bandwidth (BW) from 1.37 nm to 3.42 nm decreases the RIN. This agrees with the results of Table 1 in which the RIN behaves according to the inverse of the bandwidth. For filter F3, however, much of the power density exists far beyond the 3 dB points, so that the contribution to the RIN of the filter shape outweighs the  $BW^{-1}$  dependence. The RIN of two additional filters (not shown) having well-behaved, symmetrical shapes also followed a  $BW^{-1}$  dependence.

Figure 6.4.3 compares the RINs obtained from filter F1 when connected to EDFA1 or to EDFA2. For both combinations the RIN is very nearly constant to tens of gigahertz. The

difference in RIN of about 0.012 dB is very small. This demonstrates that filter shape alone does not determine the RIN. The similar shape of the curves occurs because each arises from the same filter. The filter bandwidth is probably narrow enough to compensate for a potentially non-zero slope of the spectral density of a typical EDFA that might occur over a wavelength interval of several nanometers around the center wavelength of the filter. If such an effect were significant, the RIN would not be constant.

### **6.5 Use of Connectors and the Effect of Losses**

The net effect of disconnecting and reconnecting the RIN standard will cause a slight variation in the total optical power transmitted down the transmission line. Connections can be made by use of either fusion splicing or fiber connectors. Since in principle the RIN is invariant under attenuation, the effect of using connectors will turn out to be very small. Thus, for convenience, we chose standard, high-quality FC/PC connectors to mate all of the fiber components composing a standard. The error due to connector mating is included in the repeatability error (section 7.1).

### **6.6 Combined Effects of Attenuation, Pump Current, and Power Spectral Density Levels**

If the spectral responsivity of the OSA is nonlinear, an error will occur in measuring different OPSD levels at the same wavelength. In principle, however, the total variation in the RIN with respect to power per bandwidth will result from the combination of a nonlinear spectral responsivity at each sampled wavelength, and any potential effect of attenuation on the RIN itself, however small. We must consider attenuation because the transmission of the optical spectrum through connectors and down the fiber transmission line of the standard may be subject to some wavelength dispersion that could, in principle, alter the RIN spectrum. Such effects should vanish to first order, but might contribute a small but finite uncertainty to the total RIN. To determine this error, we devised a scheme in which the RIN standard is attenuated over a wide range of values at various pump currents. In Figure 6.6.1, the RIN is shown over a range of attenuations from 0 dB to 10 dB. The average RIN is  $1.0296 \cdot 10^{-11} \text{ Hz}^{-1}$  (-109.87 dB/Hz) with standard deviation of  $0.0008 \cdot 10^{-11} \text{ Hz}^{-1}$  (0.003 dB/Hz). To first order, this result determines that the RIN is

nearly invariant under practical attenuation strengths that may arise from component and connector losses.

However, we must determine any potential effects of attenuation and nonlinear spectral responsivity in aggregate. The combined uncertainty will be assigned to represent an upper bound for the uncertainty due to a nonlinear spectral responsivity. Thus we determined the RIN for a variety of pump currents, attenuation levels, and intensity levels as shown in Table 2. For example, the effect of a variable attenuation could be studied with the spectral intensity held constant on the OSA screen by compensating the pump current. For other measurements the intensity level was allowed to vary. Column 3 of the Table shows the intensity relative to the maximum, which occurs at zero attenuation and maximum pump current (214 mA). Thus the maximum intensity is represented by 0 dB, while 4 dB below the maximum appears as -4 dB. Such varied conditions, again give nearly the same average value for the RIN,  $1.0297 \cdot 10^{-11} \text{ Hz}^{-1}$  (-109.87 dB/Hz) with a standard deviation of  $0.002 \cdot 10^{-11} \text{ Hz}^{-1}$  (0.008 dB/Hz), as when the intensity levels were allowed to vary. Figure 6.6.2 shows the variation in RIN with pump current at zero attenuation. The average RIN is  $1.0291 \cdot 10^{-11} \text{ Hz}^{-1}$  (-109.87 dB/Hz) and the standard deviation is  $0.0005 \cdot 10^{-11} \text{ Hz}^{-1}$  (0.002 dB/Hz). Thus the uncertainty in the RIN due to the combined uncertainties in spectral responsivity and attenuation in aggregate is indeed small.



Table 2. RIN for different values of pump current, attenuation, and intensity. To determine the effect of a nonlinear spectral responsivity, some combinations of pump current and attenuation were adjusted to give equal values of intensity on the OSA screen.

Pump current (mA)	Attenuation (dB)	Intensity relative to maximum, $I_{\max}$ (dB)	RIN ( $10^{-12}$ Hz <sup>-1</sup> )
214	0	0	10.296
214	0	0	10.286
187	0	-1	10.294
148	0	-3	10.288
137	0	-4	10.298
100.5	0	-10	10.286
214	1	-1	10.286
214	3	-3	10.304
214	4	-4	10.294
214	10	-10	10.308
187	3	-4	10.308
149	1	-4	10.288
113	3	-10	10.298
185	10	-11	10.306
186	10	-11	10.31

## 7. Total Uncertainty in RIN Standard

We determined the total uncertainty in the RIN standard from the random error or repeatability of measurements, and the contributions of the OSA parameters to the OPSD measurement. To determine the OSA's contribution to the total uncertainty we apply the propagation of errors formula to the numerical RIN formulas of the preceding section. The OSA parameters that contribute significant errors are resolution bandwidth, wavelength distortion (absolute wavelength and wavelength interval), and nonlinear spectral responsivity.

### 7.1 Repeatability Error

To determine the repeatability uncertainty, five measurements were repeated on several distinct measurement occasions over the course of several weeks. (EDFA2 with F1 was measured on eight occasions and EDFA2 with F2 was measured on four occasions.) On each occasion, the five repeated measurements were taken within a short period of time so that the measurements would be similar within the measurement occasion. On each occasion, the four connectors shown in Figure 3.1.3 were disconnected and reconnected between each of the five measurements. The repeatability uncertainty was computed as outlined in the ISO *Guide to the Expression of Uncertainty* [21]. The average RIN for the five measurements on a given day is

$$\langle RIN_i \rangle = \frac{1}{5} \sum_{j=1}^5 RIN_{ij} . \quad (7.1.1)$$

For a series of days, the average RIN is

$$\langle RIN \rangle = \frac{1}{d \cdot 5} \sum_{i=1}^d \sum_{j=1}^5 RIN_{ij} , \quad (7.1.2)$$

where d is the number of measurement occasions or days. Thus the repeatability uncertainty is

$$U_{REP} = \sqrt{\sum_{i=1}^d \frac{(\langle RIN_i \rangle - \langle RIN \rangle)^2}{d(d-1)}} \quad (7.1.3)$$

Figure 7.1.1 shows that the variance of the RIN with connector mating over the three week period is indeed very small. It is 0.002 dB and 0.005 dB for EDFA2 with filters F1 and F2, respectively.

## 7.2 Measurement Error From the OSA Parameters

In section 6.6 we showed that the combined errors which may arise from nonlinearity in the spectral responsivity, and any potential effects of attenuation, could be grouped into a single error representing an upper bound for the responsivity alone. To determine this upper bound, we varied the attenuation under constant pump current so that the spectral density level on the OSA screen varied in direct proportion to the attenuation. We computed the standard deviation of the RIN values obtained at the six attenuation levels, 0 dB, 3 dB, 6 dB, 9 dB, 11 dB, and 15 dB, from the following formula,

$$U_{LIN} = \sqrt{\sum_{i=1}^6 \frac{(RIN_i - \langle RIN \rangle)^2}{(6-1)}}, \quad (7.1.4)$$

without disconnecting or reconnecting any of the fiber components. For filters F1 and F2, the uncertainties are 0.005 dB and 0.008 dB, respectively. For example, for F1 the uncertainty in the RIN due to a nonlinear spectral responsivity has an upper bound of 0.005 dB, which will be used to estimate the total uncertainty in the RIN.

The uncertainty in RIN due to wavelength distortion was determined by applying the propagation-of-errors formula to eq (4.2.7) with  $\Delta\lambda = (\lambda_{1001} - \lambda_1)/1000$  and average wavelength error of 0.042 nm as determined from the 21 data points of Figures 5.2.1 and 5.2.2. The

resulting uncertainty is

$$U_{\lambda} = \sqrt{\left( \frac{\sum_j (\delta P_f(\lambda_j))^2}{\left( \sum_j \delta P_f(\lambda_j) \right)^2} \right)^2 \left( \frac{4008004}{(\lambda_{1001} - \lambda_1)^4} \right) (S^2(\lambda_{1001}) + S^2(\lambda_1))}, \quad (7.1.5)$$

where  $S^2(\lambda_{1001}) = S^2(\lambda_1) = (0.042 \text{ nm})^2$ , and  $j = 1, 2, \dots, n$ , where  $n$  is the number of data points.

Since  $U_{\lambda}$  is different for each RIN measurement, the  $U_{\lambda}$  used to compute the combined uncertainty is based on the maximum  $U_{\lambda}$  computed for the RIN measurements for a given filter.

The resulting uncertainties are 0.051 dB and 0.017 dB for filters F1 and F2, respectively.

The uncertainty due to variation in resolution bandwidth,  $U_{RBW}$ , was computed by applying the propagation of errors to eq (4.2.5). The propagation-of-errors formula takes the form

$$U_{RBW} = \sqrt{\left( \frac{\partial RIN}{\partial B_1(\lambda_1)} \right)^2 \text{var}(B_1(\lambda_1)) + \left( \frac{\partial RIN}{\partial B_2(\lambda_2)} \right)^2 \text{var}(B_2(\lambda_2)) + \dots + \left( \frac{\partial RIN}{\partial B_n(\lambda_n)} \right)^2 \text{var}(B_n(\lambda_n))} \quad (7.1.6)$$

But since  $\text{var}(B_1(\lambda_1)) = \dots = \text{var}(B_n(\lambda_n)) = \text{var}(B(\lambda))$ , we have

$$U_{RBW} = \sqrt{\sum_j \left( \left( \frac{\partial RIN}{\partial B_j(\lambda_j)} \right)^2 \text{var}(B(\lambda)) \right)}. \quad (7.1.7)$$

Performing the differentiation gives

$$U_{RBW} = \sqrt{A B^{-6} (B^2 C - 2B D E + D^2 F) \text{var}(B(\lambda))}, \quad (7.1.8)$$

where

$$\begin{aligned} A &= \frac{4 \cdot 2^2}{(\Delta\lambda)^2} \\ B &= \sum_j \frac{\delta P_j(\lambda_j)}{B_j(\lambda_j)} \\ C &= \sum_j \frac{\delta P_j(\lambda_j)^4}{B_j(\lambda_j)^6} \\ D &= \sum_j \frac{\delta P_j(\lambda_j)^2}{B_j(\lambda_j)^2} \\ E &= \sum_j \frac{\delta P_j(\lambda_j)^3}{B_j(\lambda_j)^5} \\ F &= \sum_j \frac{\delta P_j(\lambda_j)^2}{B_j(\lambda_j)^4} \end{aligned} \quad (7.1.9)$$

Resolution bandwidth was shown to be very nearly constant within the wavelength range of interest, so that the computations were performed at each wavelength using  $B_j(\lambda_j) = 0.045$  nm, with  $\text{var}(B(\lambda)) = 0.001$  nm as determined from the noise-equivalent bandwidth. The value of  $U_{RBW}$  used to compute the combined uncertainty is the worst-case value of  $U_{RBW}$  calculated among the RIN measurements for a given filter. These uncertainties are 0.002 dB and 0.006 dB for filters F1 and F2, respectively. The specific and combined standard uncertainties are shown in Table 3 for each filter.

### 7.3 Combined Standard Uncertainty

The RIN of the standard is the average of all RIN measurements used to compute  $U_{\text{REP}}$ . For filter F1 with 40 observations  $\langle \text{RIN} \rangle = 1.0325 \cdot 10^{-11} \text{ Hz}^{-1}$ . To compute the combined standard uncertainty of the average RIN,  $u_c$ , the four uncertainty estimates described in sections 7.1 and 7.2,  $U_{\text{REP}}$ ,  $U_{\text{LIN}}$ ,  $U_{\lambda}$ , and  $U_{\text{RBW}}$ , are added in quadrature. Since all four sources of uncertainty use measured data to compute their values (as opposed to manufacturer's specifications, for example), they are all considered Type A uncertainties. (There are no significant Type B uncertainties.) Although different amplifiers were used to quantify  $U_{\text{REP}}$  and  $U_{\text{LIN}}$ , this should not influence the uncertainty estimates.

The expanded uncertainty,  $U$ , is twice the combined standard uncertainty ( $U = 2u_c$ ), which represents an approximate 95 % confidence interval for the average RIN [22]. The combined standard uncertainty and expanded uncertainty for filters F1 and F2 are shown in Table 3. For F1, the combined standard uncertainty ( $0.014475 \cdot 10^{-11} \text{ Hz}^{-1}$ ) is 1.4 % of the average RIN ( $1.0325 \cdot 10^{-11} \text{ Hz}^{-1}$ ). The average RIN for filter F2,  $\langle \text{RIN} \rangle = 6.3712 \cdot 10^{-12} \text{ Hz}^{-1}$ , was based on 20 observations used to compute  $U_{\text{REP}}$ . The combined standard uncertainty ( $0.053564 \cdot 10^{-12} \text{ Hz}^{-1}$ ) is 0.84 % of the average RIN.

Table 3: Combined standard uncertainty in the RIN of the standard (EDFA2 with filters F1 and F2).

<b>EDFA2 + F1</b>	<b>Uncertainty type (A or B)</b>	<b>Standard uncertainty in 1/Hz</b>	<b>Standard uncertainty in dB</b>
$U_{REP}$	A	$0.000561 \cdot 10^{-11}$	0.002
$U_{LIN}$	A	$0.001180 \cdot 10^{-11}$	0.005
$U_{\lambda}$	A	$0.012315 \cdot 10^{-11}$	0.051
$U_{RBW}$	A	$0.000419 \cdot 10^{-11}$	0.002
<b>Combined, <math>u_c</math></b>	-	$0.014475 \cdot 10^{-11}$	0.06
<b>Expanded, U</b>	-	$0.029 \cdot 10^{-11}$	0.12
<b>EDFA2 + F2</b>			
$U_{REP}$	A	$0.0068325 \cdot 10^{-12}$	0.005
$U_{LIN}$	A	$0.011804 \cdot 10^{-12}$	0.008
$U_{\lambda}$	A	$0.025354 \cdot 10^{-12}$	0.017
$U_{RBW}$	A	$0.009581 \cdot 10^{-12}$	0.006
<b>Combined, <math>u_c</math></b>	-	$0.053564 \cdot 10^{-12}$	0.036
<b>Expanded, U</b>	-	$0.10713 \cdot 10^{-12}$	0.072

## 8. Achieving the Poisson Limit

For an optical field at wavelength  $\lambda$  and optical power  $P_o$ , the Poisson RIN is

$$R_p(\lambda) = R_p = \frac{2hc}{\lambda P_o} \approx \text{constant} , \quad (8.1)$$

where  $c$  is the speed of light and  $h$  is Planck's constant. To achieve the Poisson limit we recall that any optical source can be rendered Poisson-limited by sufficient attenuation [23]. This occurs because the Poisson RIN increases with attenuation while the excess RIN remains invariant. Thus for applications of low-power lasers, the Poisson limit may be useful if the excess RIN is very small and there is sufficient optical power available after attenuation to meet the power requirements. However, the true Poisson limit is reached when the ratio of excess to Poisson RIN

approaches zero.

A Poisson-limited source offers two distinct advantages over that of a low-excess-RIN source. First, the Poisson RIN is manifest in the electrical detection circuit as the simple quantity  $2q/i$ . Second, the calibration of a RIN system can be performed with a Poisson-limited laser without knowing the RIN explicitly, as will be shown in the following section. To establish a RIN standard, we need not achieve the true Poisson limit, but require only that the ratio of excess to Poisson RIN be small. Through attenuation we constrain this ratio to fall within some fixed value, and thus limit the error it contributes to a RIN system calibration.

### **8.1 The DFB Laser of the Secondary Method Has Nearly Poisson-Limited RIN**

In this section we apply eq (8.1) to a series of RIN measurements under attenuation to show that the RIN of our laser is nearly Poisson-limited, and contributes only a very small error in the calibration of our RIN measurement system. Calibration of the RIN system yields a frequency-dependent calibration function that we call Kappa. Kappa is a dimensionless quantity (precisely defined in section 9) whose magnitude is not required for the present analysis. To proceed, we first compare graphs of Kappa obtained from measurements using the DFB laser at several attenuation levels for which optical power ranged from one half mW to 7 mW. Figures 8.1.1 and 8.1.2 show the frequency dependence of Kappa for the various attenuation levels. In Figure 8.1.1 the levels are 10, 12, and 15 dB based on a single sweep of the ESA. In Figure 8.1.2 the levels are 10, 13, and 16 dB, with each curve obtained from an average of nine sweeps. This gives a smaller spread in the data. The data overlap for all but the 10 dB curve in Figure 8.1.2, which sits slightly below its neighbors. Thus the overlap of the 15 and 12 dB levels, and the 16 and 13 dB levels, indicates that the RIN should be very close to the Poisson limit over the entire bandwidth. At 10 dB, however, the optical power is considerably greater, the Poisson RIN smaller, so that the ratio of excess to Poisson RIN may be too large to have achieved the Poisson limit. Since all calibrations made with the laser are at 17 dB attenuation, this result for the Poisson limit should still hold.

Figure 8.1.3 shows the rf-noise power (in arbitrary units) at 400 MHz plotted versus dc voltage. Since Poisson noise power manifests in the electrical detection circuit as  $2qV$  (where  $q$  is



electron charge and  $V$  is voltage), the data should yield a straight line [24]. (The noise power is  $2qV\Delta B$ , which is  $2qV$  in a 1Hz bandwidth.) The voltage values range from 9.39 to 23.66 mV, with corresponding attenuations from 18 to 14 dB. The first curve is a second-order polynomial fitted to all data points. The second curve is a linear fit of all points except  $V = 23.66$  mV (which corresponds to only 12 dB attenuation). The two curves rapidly converge to a straight line with increasing attenuation (decreasing voltage). At a voltage of 11.82 mV, where the attenuation is 17 dB, the curves are straight lines. This is the normal operating regime for this standard. A second-order polynomial fit of all points except  $V = 23.66$  mV yields a coefficient of very nearly zero (slightly negative) for the second-order term. Thus the excess RIN component is too small to resolve.

A simple argument can be given that further supports our results, and is based on the manufacturer's specification of the excess RIN ( $\leq -172$  dB/Hz at the operating current of 169.44 mA, where power output is 27.82 mW). At this current and 17 dB attenuation, accounting for all losses, the optical power incident on the detector is 0.275 mW. Since the Poisson RIN in the photodetector circuit increases by  $1/\eta$ , where  $\eta = 0.77$  is the detector quantum efficiency, the equivalent Poisson RIN at an optical power of 0.212 mW from eq (8.1) is  $-149.2$  dB/Hz. Since the excess RIN remains  $\leq -172$  dB/Hz, the ratio of excess to Poisson RIN would be  $\leq 0.005$  ( $\leq 0.022$  dB).

## 9. RIN System Calibration Using the Standard and the Laser

To validate the RIN standard and associated MAP, we developed two distinct methods, each of which uses a precision RIN source, to separately calibrate our RIN measurement system. We evaluate both methods by comparing calibration results. Because the photon number distributions differ for the two methods, so too will their calibration functions. By formulating the optical RIN of each source before it enters the RIN system and the electrical RIN measurement inside, we derive an equation that relates the response of the system to the two sources. First, we note a pair of simplifying distinctions between the methods. For the standard, we can consider the amplitude fluctuations to be of purely second order, that is, devoid of Poisson light, as this

component is much smaller than the EDFA's amplified spontaneous emission. For the DFB laser, the RIN can be considered purely Poisson, as shown previously. Figure 9.1 demonstrates how each method is applied separately to the RIN measurement system.

### 9.1 Derivation of the Calibration Equations For the Standard and Secondary Methods

In this section we derive the calibration equations (Kappas, or frequency-dependent calibration functions) that govern the response of our RIN system to the input RIN of the standard and the Poisson laser. Let  $\delta P_a$  and  $\delta P_p$  be the rf noise measured on the ESA from the EDFA + F and the laser, and  $P_a, P_o$  the corresponding electrical dc powers, respectively. Let  $R_a$  be the RIN calculated from the optical spectrum of the EDFA + F as measured on the OSA, and  $\kappa_a(\omega)$  and  $\kappa_p(\omega)$  the system calibration functions from the EDFA + F and the laser, respectively. Then for the EDFA + F we must have

$$R_a(\omega) = R_a = \kappa_a(\omega) \cdot \frac{\delta P_a(\omega)}{P_a} \approx \text{constant} . \quad (9.1.1)$$

Solving for  $\kappa_a$  gives

$$\kappa_a(\omega) = \frac{R_a \cdot P_a}{\delta P_a(\omega)} . \quad (9.1.2)$$

For the laser,

$$R_p = \kappa_p(\omega) \cdot \frac{\delta P_p(\omega)}{P_p} = \frac{2hc}{\lambda P_o} \approx \text{constant} , \quad (9.1.3)$$

so that

$$\kappa_p(\omega) = \frac{2hc}{\lambda P_o} \cdot \frac{P_p}{\delta P_p(\omega)}, \quad (9.1.4)$$

where  $2hc/\lambda P_o$  is the Poisson RIN of the laser.

## 9.2 Equivalence of the Calibration Functions

To derive an exact expression equating the calibration functions we note that the Poisson RIN of the laser increases in the electrical detection circuit by an amount  $1/\eta$ . Therefore an equivalent optical RIN for the laser that would yield a Kappa equivalent to that for the standard, with all other conditions kept constant, is

$$\frac{R_p}{\eta} = \kappa_p(\omega) \cdot \frac{\delta P_p(\omega)}{P_p}, \quad (9.2.1)$$

where now  $\kappa_a = \kappa_p$ . Solving for  $\kappa_p$  gives

$$\kappa_p(\omega) = \frac{R_p \cdot P_p}{\eta \cdot \delta P_p(\omega)}. \quad (9.2.2)$$

The photocurrent in the electrical circuit is  $i = \rho P_o = \eta q P/h\nu$ , where  $h$  is Planck's constant,  $q$  is the electron charge, and  $\rho$  and  $\eta$  are the responsivity and quantum efficiency of the photodetector, respectively. The dc voltage is  $V = ir$ , where  $r$  is resistance. Substituting these expressions for current and eq (9.1.3) for the Poisson RIN, the quantum efficiency cancels and we obtain

$$\kappa_p(\omega) = \frac{2qV}{\delta P_p(\omega)}. \quad (9.2.3)$$

Therefore,

$$\kappa(\omega) = \frac{R_a \cdot P_a}{\delta P_a(\omega)} = \frac{2qV}{\delta P_p(\omega)}, \quad (9.2.4)$$

where we dropped the subscripts on Kappa. From this analysis it is clear that  $\kappa_p$  can be determined without knowledge of the laser RIN or the quantum efficiency of the photodetector (measured at 0.77 at the operating wavelength of 1555.9 nm). Note that the variation of Kappa with frequency for either method is directly proportion to the frequency response of the RIN system. As such, either method might be used to measure the frequency response of high-speed photoreceivers. In the next section we use these results to compare the calibration functions obtained from actual calibrations of our RIN measurement system.

## 10. Two Methods Applied to the NIST RIN System Give Similar Results

To evaluate the accuracy of the RIN standard we used it to calibrate our rf (electrical) RIN measurement system, and compared the results with those obtained using the laser. Such a comparison should help determine the validity of the RIN standard with respect to the secondary method, in that each method, when applied separately to the RIN system, should yield similar results. From this we can predict how a typical RIN system will respond to the RIN standard, and how well the results agree with any conclusions drawn about either method separately. It should also provide a framework for comparing the statistical uncertainties obtained from each method.

### 10.1 Quantitative Comparison of Calibration Results from the Two Methods

Since we seek to establish a MAP that allows replacement of various components composing the standard and the RIN system, we performed calibrations using a variety of components for the standard, and compared results. Among these are the six combinations that arise from the two EDFAs and the three filters discussed previously (section 6.4). Use of a single Poisson-limited laser for the secondary method is justified because the theory and measurement of Poisson light

are well established, so that we need only determine that the laser's RIN obeys Poisson statistics. To compare the standard with the laser we used eq (9.24), which equates their calibration functions.

First we obtained Kappa for the three filters of different shape and bandwidth using EDFA2. The results are shown in Figure 10.1.1 for bandwidths of 1.32, 1.37, and 3.42 nm. The shape and overlap of the three curves confirms that our calculation of the RIN scales with filter bandwidth and shape as expected from theory. The similarity in all three Kappas indicates that calibration of the RIN system is independent of the magnitude of the RIN and the shape of the filter. Next we compared the laser with filter F2 using both EDFA1 and EDFA2. The results shown in Figure 10.1.2 are again similar. Note that measurements were taken sequentially in the shortest time reasonable to duplicate experimental conditions. When a set of calibrations was performed using different EDFAs, a matching set was performed with the laser, reinforcing the comparison of the two methods.

To quantify the calibration results as a comparison of methods between the laser and combinations of different components intended to compose a valid standard, we determined the simple average of the difference between Kappas recorded at each frequency over the spectrum. Let  $\kappa_{a,i}$  and  $\kappa_{p,i}$  represent Kappa of the standard and the laser at the  $i$ th frequency  $f_i$ , respectively, and  $D_i$  is the difference between Kappas,  $D_i = \kappa_{a,i} - \kappa_{p,i}$ . Then the average difference,  $Z$ , is obtained by summing over the 601 points in a spectrum,

$$Z = \frac{\sum D_i}{601} = \frac{\sum (\kappa_{a,i} - \kappa_{p,i})}{601} \quad (10.1.1)$$

Figure 10.1.3 shows a typical distribution of differences obtained for the standard (EDFA1 + F2) and the laser. The differences range from -1 to +1 dB, with an average difference of 0.058 dB. The standard deviation of the differences is 0.3 dB, which illustrates the rather large fluctuations that are characteristic of such rf noise spectra.

In Table 4 we compare calibration results from the laser with various combinations of

components that could form a valid standard. The sources compared are listed in column 1 along with the date of the experiment. The first and second numbers in column 2 represent the average difference of the Kappas without and with the ESA scale fidelity correction (SFC), respectively (see Appendix A). Column 3 shows the standard deviation of the average differences of column 2, again, without and with the scale fidelity correction. We list some of the comparisons and their meanings. Kappa from each of the two amplifiers was determined using all three filters, F1, F2, and F3, and compared with Kappa from the laser on different days. Thus we might compare Kappa of EDFA 1+ F1 with Kappa of DFB (experiment of April 27). We also compare Kappa among various combinations of EDFAs and filters. Thus we compare EDFA1 + F2 with EDFA2 + F2 (experiment of April 20), EDFA1 + F1 with EDFA1 + F2 (April 29) , and the laser at two different times: DFB(2) with DFB(3) (experiment of April 13). The behavior for all comparisons is very similar, with the smallest variation occurring for two different EDFAs using the same filter (April 23), or the laser with itself (April 23).

We performed a number of comparisons using EDFA1 and EDFA2 with all three filters in which we calculated the average of the average difference of the two Kappas compared. For example, we compared each EDFA + filter with the other EDFA using the same filter. We also compared the laser with different combinations of EDFAs and filters. The results show good agreement at all frequencies when averaged. The average differences between single data sets, as shown in Table 4, are quite small.

Table 4. Comparison of the standard with the Poisson laser; other similar comparisons.

Combinations of sources and filters compared	Z (eq 10.1.1), in dB		Standard deviations of the differences, D, in dB.	
	without,	with SCF	without,	with SCF
<i>5/3/99; F2 only</i>				
EDFA1 + F2 with EDFA2 + F2	0.077,	0.049	0.337,	0.355
EDFA1 + F2 with DFB	0.091,	0.108	0.301,	0.311
EDFA2 + F2 with DFB	0.013,	0.082	0.343,	0.359
<i>4/29/99; F1 and F2</i>				
EDFA1 + F2 with EDFA2 + F2	-0.041,	-0.107	0.356,	0.372
EDFA1 + F2 with DFB(2)	0.143,	0.161	0.305,	0.316
EDFA2 + F2 with DFB(2)	0.184,	0.268	0.34,	0.358
EDFA1 + F1 with EDFA2 + F1	-0.043,	-0.054	0.212,	0.215
EDFA1 + F1 with DFB(1)	0.142,	0.064	0.246,	0.249
EDFA2 + F1 with DFB(1)	0.185,	0.118	0.251,	0.254
EDFA1 + F1 with EDFA1 + F2	0.11		0.279	
EDFA2 + F1 with EDFA2 + F2	0.112		0.314	
DFB(1) and DFB(2)	0.112		0.295	
<i>4/27/99; F1 only</i>				
EDFA1 + F1 with EDFA2 + F1	0.088,	0.079	0.211,	0.214
EDFA1 + F1 with DFB	0.12,	0.042	0.255,	0.258
EDFA2 + F1 with DFB	0.033,	-0.036	0.246,	0.25
<i>4/23/99; F1 and F3</i>				
EDFA1 + F3 with EDFA2 + F3	- 0.0066,	-0.036	0.292,	0.30
EDFA1 + F3 with DFB(3)	0.108,	0.094	0.291,	0.299
EDFA2 + F3 with DFB(3)	0.115,	0.13	0.301,	0.311
EDFA1 + F1 with EDFA2 + F1	0.041,	0.041	0.195,	0.198
EDFA1 + F1 with DFB(1)	0.188,	0.113	0.245,	0.248
EDFA2 + F1 with DFB(1)	0.146,	0.071	0.246,	0.249
EDFA1 + F1 with EDFA1 + F3	0.074		0.232	
EDFA2 + F1 with EDFA2 + F3	0.025		0.252	
DFB(1) and DFB(3)	0.0061		0.285	

Combinations of sources and filters compared	Z (eq 10.1.1), in dB		Standard deviations of the differences, D, in dB.	
	without,	with SCF	without,	with SCF
4/20/99; F2 only				
EDFA1 + F2 with EDFA2 + F2	-0.095,	-0.202	0.31,	0.327
EDFA1 + F2 with DFB	-0.111,	-0.147	0.286,	0.292
EDFA2 + F2 with DFB	-0.016,	-0.0014	0.343,	0.333
4/19/99; F3 only				
EDFA1 + F3 with EDFA2 + F3	-0.015,	-0.049	0.263,	0.27
EDFA1 + F3 with DFB	0.132,	0.103	0.263,	0.269
EDFA2 + F3 with DFB	0.147,	0.152	0.27,	0.279
4/16/99; F1 only				
EDFA1 + F1 with EDFA2 + F1	0.012,	-0.108	0.157,	0.164
EDFA1 + F1 with DFB	0.08,	-0.001328	0.186,	0.188
EDFA2 + F1 with DFB	0.068	0.000864	0.188,	0.191
4/13/99; F2 and F3				
EDFA1 + F2 with EDFA2 + F2	-0.028,	-0.074	0.331,	0.349
EDFA1 + F2 with DFB(2)	0.053,	0.058	0.293,	0.302
EDFA2 + F2 with DFB(2)	0.08,	0.143	0.334,	0.35
EDFA1 + F3 with EDFA2 + F3	-0.0042,	-0.056	0.286,	0.295
EDFA1 + F3 with DFB(3)	0.103,	0.076	0.265,	0.271
EDFA2 + F3 with DFB(3)	0.099,	0.131	0.29,	0.301
EDFA1 + F2 with EDFA1 + F3	0.105		0.268	0.333
EDFA2 + F2 with EDFA2 + F3	0.073		0.28	
DFB(2) and DFB(3)	0.051			



Table 5. Relative stability of EDFA1 and EDFA2 with respect to the Poisson laser.

	Average of the Z's (dB)	Average of standard deviations (dB)
EDFA1 + F <sub>x</sub> with DFB	0.088	0.046
EDFA2 + F <sub>x</sub> with DFB	0.103	0.077

### 10.2 Relative Stability of Two Different EDFAs With Respect to the Poisson Laser

From the data in Table 4, we can compare the accuracy and relative stability of EDFA1 and EDFA2 with respect to the Poisson laser. The averages for each EDFA were made over all comparisons with the laser. Specifically, we found the average of the average difference of Kappas for a specific EDFA with any of the three filters as compared with the corresponding Kappa from the DFB laser. A comparison of EDFA1 with laser will have the following entries from Table 4 - column 2, for computing this average: EDFA1 + F2 with DFB (5/3, 4/29, 4/20), EDFA1 + F1 with DFB (4/29, 4/27, 4/23), EDFA1 + F3 with (4/23, 4/19, 4/13). Similar entries occur for comparisons of EDFA2 with the laser. We used the second set of numbers in column 2, which accounts for the ESA scale fidelity correction. The results are shown in Table 5, where F<sub>x</sub> represents filters F1, F2, and F3. EDFA1 is slightly more stable, with an average of 0.088 dB, while EDFA2 (the standard) has an average of 0.103 dB. These averages disagree by 0.015 dB, which is quite small. Recall that we chose EDFA2 for the standard because of its semi-ruggedness and ease of use.

We note that in determining Kappa the ESA's noise floor is subtracted. This is an arbitrary procedure because the noise floor, which is averaged in the measurement process, is the same for both the standard and the laser. Of importance is that we be consistent in how we define the RIN system's response to the standard and the laser.

### 10.3 Methods Compare Favorably Under Use of Variance Analysis

As was shown in section 9.2 above, Kappa from the laser can be precisely determined without explicit knowledge of the laser's RIN. Thus we can compare calibration results from the standard

and the laser by measuring their calibration functions. Our main objective in this section is to verify that the variations in their calibration functions are similar. Again, all calibrations are performed using the NIST RIN measurement system.

During a one-day period, we determined Kappa using both the standard and the laser as a pair of sequential measurement sets taken in the least time possible (~2 min); this is the time needed to store the data for the standard, disconnect the standard, connect the laser, and collect the new data. This insures nearly identical environmental conditions (such as temperature and background rf fields) for the two methods. Stray rf signals can appear unpredictably in a data spectrum, for example from mobile telephone sources, and their magnitude may vary during the time of a measurement. They must be averaged out by manual inspection of the data. (The ESA data are averaged from nine sweeps, which takes about 20 s).

Figures 10.3.1, 10.3.2, and 10.3.3 show the data from four different days for Kappa of EDFA1 + F1, EDFA2 + F1, and the laser, respectively. The different symbols represent the four measurement occasions. The distribution of Kappa with frequency is fairly repeatable within each method, and follows a similar pattern when comparing methods. Figure 10.3.4 compares the average value of Kappa for EDFA1 + F1 with that of the laser, where the Kappas at each frequency are the calculated averages of the same four data points from Figures 10.3.1 and 10.3.3. Figure 10.3.5 compares the average value of Kappa for EDFA2 + F1 with that of the laser, where the Kappas at each frequency are the calculated averages of the same four data points from Figures 10.3.2 and 10.3.3. Kappa for the laser is slightly lower than that of either EDFA using F1.

To assess the variation in Kappa for both methods, we calculated the normalized standard deviation of the four observations at each frequency. Scatter plots of the data are shown in Figures 10.3.6 and 10.3.7 for the laser compared with EDFA1 + F1 and EDFA2 + F1, respectively. The data indicate that the two independent methods give similar standard deviations over the entire frequency range, indicating that they are comparable.

#### **10.4 F-ratio Test Yields Similarity in the Variability of the Calibration Functions**

We performed a statistical F-test to compare the variability in Kappa between the two

methods. This test computes the ratio of the variances for the two methods and compares this ratio to critical values from an F-table [25]. To apply the test we define the ratio

$$F = \frac{S_L^2}{S_A^2}, \quad (10.4.1)$$

where  $S_L^2$  and  $S_A^2$  are the sample variances for Kappa of the laser and standard, respectively. If the variances obtained from the two methods are very similar, then F will not be too large or too small. Specifically, if F is greater than the  $100(1 - a/2)^{\text{th}}$  percentile of the F distribution, or less than the  $100(a/2)^{\text{th}}$  percentile, the variances will be considered significantly different. The value, “a,” is the probability of incorrectly concluding that the variation in Kappa for the two methods is different. Usually “a” is a small number since we want the probability of making an error to be small. The critical values from the F table are  $F_{1-a/2; 3, 3}$  and  $F_{a/2; 3, 3}$ , where the values 3 and 3 are the respective degrees of freedom for  $S_L^2$  and  $S_A^2$ . If  $a = 0.05$ , then the critical values are  $F_{0.975; 3, 3} = 15.44$  and  $F_{0.25; 3, 3} = 0.07$ .

To compare methods, we apply the F-ratio test at each frequency. Because the sample sizes are identical for each method, the critical values are the same for each test. Figure 10.4.1 shows the distribution of F-ratios with frequency by comparing the laser with EDFA1 + F1. The two horizontal reference lines on the plot represent the critical values for the F test when  $a = 0.05$ . The majority of the F ratios lie within the critical values, indicating that the two variances are not statistically different. The F tests at each frequency confirm that the variation in Kappa is similar for the two methods studied.

We repeated the F-test using EDFA 2 + F1. The results shown in Figure 10.4.2 are equivalent to those obtained for EDFA1, again confirming that the variation in Kappa is similar for the two methods. We expect such good agreement because the RIN of both the laser and the standard (using either EDFA) are both known and constant over the entire frequency band, and the relationship between their Kappas was precisely determined from physical laws.

## **11. Maintaining a Measurement Assurance Program**

### **11.1 Maintaining the RIN Standard**

To insure the accuracy and stability of the RIN standard with time, the RIN will be determined before it is sent to a customer, and again when it is returned. The customer will need only to connect and disconnect the component chain at a single connector. However, because the standard must be accurate and valid under substitution of different components, we will perform any necessary measurements to account for disconnection and reconnection of the components as deemed relevant for its upkeep. Thus a reference database will be kept to evaluate the long-term accuracy and stability of the standard.

For example, we began this database by performing a study using EDFA2 with filters F1 and F2. Eight sets of RIN measurements were taken on seven different days over the course of several weeks, each set composed of five repeated measurements. Filter F1 was measured on eight occasions, while filter F2 was measured on four occasions. The five repeated measurements were taken within a short period of time so that they would be similar within the measurement occasion. On each occasion the four connectors shown in Figure 3.1.3 were disconnected and reconnected between each of the five measurements. This relatively small data set, shown in Figure 7.1.1, fails to indicate the presence of a long-term trend. However, the variability within a day's measurements appears to be decreasing. Additional measurements will be required to monitor the performance of the standard, and validate its long term stability.

### **11.2 Substitution of Components**

Since components composing the standard and the NIST RIN measurement system, such as the EDFA or the ESA, respectively, can fail and need replacement, it is our intention that this MAP be validated to account for such changes. We believe that the net effect of any required changes in components has been accounted for based on our thorough development of the theory and the precision with which the measurements were performed. Because both the RIN of the standard as well as the Poisson-limited laser are constant in frequency out to tens of gigahertz, this MAP should be extendable to such higher frequencies with little or no additional certification.

Also, since the intensity noise of the Poisson-limited laser is predictable and stable, and its RIN is well known and historically accurate, it too can be considered a RIN standard. However, because it is not as field employable, it is most useful as a laboratory standard.

---

We are especially grateful to Wayne Itano for carefully verifying the mathematical expressions for the RIN of thermal light. We thank the Electronics and Electrical Engineering (EEL) Measurement Committee, Richard Jones (chairman), John Kitching, and Wayne Itano for evaluating various scientific and technical aspects of the manuscript. The first author thanks Paul Hale for many stimulating discussions related to this work, and for his general interest in the subject matter. Jack Dupre of Agilent Technologies provided insight on calibration methods for optical spectrum analyzers. Jack Wang discussed statistical tests for comparing two independent methods.

## 12. References

- [1] Agrawal, G.P.; Dutta, N.K. *Semiconductor Lasers*. New York: Van Nostrand Reinhold; pp. 258-269; 1993.
- [2] Obarski, G.E.; Jones, R.D. Relative Intensity Noise Correlates with Beam Profile in an LP11 Mode Vertical-Cavity Surface-Emitting Laser, in Conference on Lasers and Electro-Optics, Vol. 11, 1997 OSA Technical Digest Series, Washington, D.C.: Optical Society of America, pp. 228-229, 1997.
- [3] Coldren, L.A.; Corzine, S.W. *Diode Lasers and Photonic Integrated Circuits*. New York: John Wiley; pp. 221-236; 1995.
- [4] Petermann, K. *Laser Diode Modulation and Noise*. Norwell, Massachusetts: Kluwer Academic Publishers; pp. 157-160; 1991.
- [5] Agrawal, G.P. *Fiber-Optic Communication Systems*. New York: John Wiley; pp. 217, 306; 1992.
- [6] Saleh, B.E.A.; Teich, M.C. *Fundamentals of Photonics*. New York: John Wiley; pp. 405, 489; 1991.
- [7] Goodman, J.W. *Statistical Optics*. New York: John Wiley; pp. 472-477; 1985.
- [8] Yariv, A. *Optical Electronics in Modern Communications*. New York: Oxford University Press; pp. 449-454, 703-722; 1997.
- [9] Obarski, G.E.; Hale, P.D. How to Measure Relative Intensity Noise in Lasers. *Laser Focus World*, pp. 273-277; May 1999.

[10] Becker, P.C.; Olsson, N.A.; Simpson, J.R. *Erbium-Doped Fiber Amplifiers—Fundamentals and Technology*. New York: Academic Press, pp. 258-263, 1999.

[11] Willems, F.W.; Van der Plaats, J.C. Optical Amplifier Noise Figure Determination by Signal RIN Subtraction, in Technical Digest—Symposium on Optical Fiber Measurements, Day, G.W.; Franzen, D.L.; Hickernell, R.K., eds. NIST Special Publication 864, pp. 7-9; Sept 1994.

[12] Willems, F.W.; Van der Plaats, J.C. Experimental Demonstration of Noise Figure Reduction Caused by Nonlinear Photon Statistics of Saturated EDFAs. *IEEE Photonics Technology Letters*, Vol. 7, No. 5, pp. 488-490, May 1995.

[13] Movassaghi, M.; Jackson, M.K.; Smith, V.M.; Hallum, W.J. Noise Figure of Erbium-Doped Fiber Amplifiers in Saturated Operation. *Journal of Lightwave Technology*, Vol. 16, No. 5, pp. 812-817, May 1998.

[14] Movassaghi, M.; Jackson, M.K.; Smith, V.M.; Young, J.F.; Hallum, W.J. Accurate Frequency Resolved Measurement of EDFA Noise Figure. *Optical Amplifier Conference Digest*, British Columbia; paper # TuD1-1; pp. 130-133; July 1997.

[15] Baney, D.M.; Sorin, W.V.; Newton, S.A. High-Frequency Photodiode Characterization Using a Filtered Intensity Noise Technique. *IEEE Photonics Technology Letters*, Vol. 6, No. 10, p.1258; October 1994.

[16] Baney, D.; Sorin, W. Broadband Frequency Characterization of Optical Receivers Using Intensity Noise. *Hewlett-Packard Journal*, pp. 6-12, February 1995.

[17] Mandel, L.; Wolf, E. *Optical Coherence and Quantum Optics*. New York: Cambridge University Press; 1995.

[18] Private discussions with L. Mandel; June, 1999. Mandel acknowledges an error of a factor of two in eq (9.8.26) of their text; see reference 17. The factor of  $\frac{1}{2}$  in front of the middle integral should be removed.

[19] Mandel, L. Fluctuations of Light Beams. *Progress in Optics*, Vol. 2, Wolf, E., ed. New York: North-Holland Publishing Company—Amsterdam; p. 200; 1963.

[20] Private conversation with A. Girard. EXFO Fiber Optic Test Equipment Corp.; January 1999.

[21] Guide to the Expression of Uncertainty in Measurement. Section H-5: Analysis of Variance; International Organization for Standardization, pp. 85-87; 1993.

[22] Taylor B.N.; Kuyatt, C.E. *Guidelines for Evaluating and Expressing the Uncertainty of NIST Measurement Results*. NIST Technical Note 1297; 1994.

[23] Machida, S.; Yamamoto, Y. Quantum-Limited Operation of Balanced Mixer Homodyne and Heterodyne Receivers. *IEEE Journal of Quantum Electronics*, Vol. QE-22, No. 5, p. 617-624; May 1986.

[24] Cox, M.C.; Copener, N.J.; Williams, B. High sensitivity precision relative intensity noise calibration standard using low noise reference laser source. *IEE Proceedings, Science and Measurement Technology*, Vol. 145, No. 4, pp. 163-165; July 1998.

[25] Box, G.E.P.; Hunter, W.G.; Hunter, J.S. *Statistics for Experimenters*. New York: John Wiley; pp. 117-123; 1978.



## Appendix A. Calibration of the Electrical Spectrum Analyzer; Scale Fidelity Correction

A complete calibration of the rf spectrum analyzer is not necessary because all but one function setting that contributes to a measurement is included in Kappa. Not included, however, is a scale fidelity factor that accounts for the vertical position of the noise signal on the screen of the ESA. RIN measurements made for which the rf amplitude noise has different magnitudes must account for this factor. Like Kappa, this factor also has a frequency dependence.

We computed the scale fidelity factor for our ESA using the procedure illustrated in Figure A1. An rf signal generator was set at a predetermined power level with oscillation frequency of 500 MHz. The power was precisely measured with an rf power meter. A 10 dB attenuator was then inserted into the transmission line and the power recorded, yielding a magnitude of 10 dB for the attenuation. This procedure of measuring the power with and without the attenuator was then applied to the electrical spectrum analyzer. Connector losses were carefully accounted for, and control settings were the same as for the RIN measurements, including the position of the signal on the screen. The vertical scale was set at 5 dB per vertical division. Measurement of the rf signal with and without the 10 dB attenuator occurred at a vertical separation of 9.67 dBm on the screen. Thus for one division on the screen, the uncertainty in noise power due to the scale fidelity was  $(10 - 9.7)/2 = 0.15$  dB. (The manufacturer's specification for the ESA is that the amplitude error can be no greater than 0.7 dB over the 10 divisions that compose the screen.)

Note that the uncertainty in ESA resolution bandwidth (RBW) is included in the calibration function; thus it need not be determined separately. Of prime importance, however, is that a calibration holds true only for a given group of ESA sweep control settings, such as RBW, sweep time, internal attenuation, etc. Our calibration method neglects only error due to the vertical scale reading, or scale fidelity factor. A number of calibrations performed at different settings of RBW or sweep time etc. would give calibration curves of slightly different magnitude, but similar shape at each setting.

We now determine a scale fidelity correction for comparing signals of varying magnitude, such as occurs for Kappa from the amplifier compared with Kappa from the laser (see section 9.2 and eq (10.1.1)). The direction of this correction, which is applied at each frequency separately, is to expand the difference between the two noise powers on the screen. If the difference between noise powers is  $\delta P_1 - \delta P_2$  (at the same frequency) and S is the correction, then

$$S_1 = \frac{\delta P_1}{\delta P_1 + 0.03 \cdot (\delta P_1 - \delta P_2)}, \quad (\text{A.1})$$

The corrected Kappa at each frequency is

$$\kappa_{1,cor} = \frac{\kappa_{1,un} \cdot \delta P_1}{\delta P_1 + 0.03 \cdot (\delta P_1 - \delta P_2)}, \quad (\text{A.2})$$

where the subscripts *cor* and *un* represent the corrected and uncorrected Kappas, respectively. This is a most general formula, in which  $\delta P_1$  can be greater or less than  $\delta P_2$ . If it is greater, the corrected Kappa increases. If it is less, the corrected Kappa decreases.

## Appendix B. Addition of RIN

Although RIN is often represented in logarithmic units, it must be added directly in linear units. A good example is the subtraction of Poisson RIN from total RIN to yield excess RIN. If these quantities are specified in logarithmic units, each must be converted to linear numbers, then the subtraction performed. The resulting real number can be converted back to logarithmic form. Recall that the RIN is defined as the sum of the Poisson and the excess RIN (sections 2.1, 2.3). Then a laser emitting 0.5 mW optical power (which has Poisson RIN of -153 dB/Hz) and having a RIN of -152.2 dB/Hz will have an excess RIN of -160 dB/Hz. But 10 mW of optical power (-166 dB/Hz of Poisson RIN) with the same excess RIN will have a RIN of -159 dB/Hz.

## Appendix C. Information for Applying the RIN Standard

A calibration should be performed with the user's electrical spectrum analyzer in a fixed state of function settings. If a setting is changed to accommodate a noise spectrum of different magnitude, a new calibration curve must be obtained for the appropriate conditions.

As an example, we give some information on the ESA used in the NIST RIN system. Scale fidelity can add an uncertainty of 0.075 dB per vertical division, and which requires that we shift the calibration curve down by this amount. Thus measuring the RIN of two lasers of noise spectra three divisions apart on the screen, would result in an uncertainty in their calibration curves that would shift them apart by up to 0.225 dB. But changing reference levels so that the second spectra would fall at the same vertical position on the screen would add an even greater uncertainty of 1 dB for our ESA. Changing RBW settings would add an error of 0.5 dB.

**Appendix D: Sample MAP Certificate**

**U.S. DEPARTMENT OF COMMERCE  
NATIONAL INSTITUTE OF STANDARDS AND TECHNOLOGY  
ELECTRONICS AND ELECTRICAL ENGINEERING  
LABORATORY  
Boulder, Colorado 80303**

**MEASUREMENT ASSURANCE PROGRAM (MAP)**

**for**

**Spectral Density of Relative Intensity Noise**

**for**

**Customer**

**AaBbCc Corp.**

**Address**

**Calibration Summary**

This report summarizes the measurement results for the spectral density of Relative Intensity Noise (RIN) of the NIST transfer standard. The standard is calibrated over the 0.1 GHz to 1.1 GHz frequency range. However, the spectral density of the RIN (from now on called simply the RIN) is practically constant up to several tens of gigahertz. The transfer standard is an erbium-doped fiber amplifier (EDFA) to which is coupled a linear polarizer (P) followed by a narrowband filter (F) (represented as EDFA + P + F in Figure D1). The EDFA has a built-in optical isolator to ensure that the amplified-spontaneous emission (ASE) that it emits is free from potential multiple interference effects such as ripple. High-quality FC/PC connectors and single-mode fiber are used throughout.

Folder No. and NIST ID: xx and yy

Date of Report: March 1, 2000

Reference: P.O. No. Mmm, 2/3/00

The RIN of the standard is determined from measurements of the optical power spectral density (OPSD) it emits as measured by a high resolution, grating-type, optical spectrum analyzer (OSA). The RIN is proportional to the autocorrelation of the measured OPSD. Thus the uncertainties that contribute to the RIN are the repeatability and those that arise from the OSA parameters involved in the measurement.

The reported results are the average of the NIST calibration measurements made before and after shipment to the participant, and are summarized in Table I in linear as well as logarithmic units.

**Table D1.** RIN of the transfer standard (based on 40 RIN measurements).

Frequency range	RIN (EDFA + P + F)		Expanded uncertainty	
	1/Hz	dB/Hz	1/Hz	dB/Hz
0.1-1.1 GHz	$1.0325 \cdot 10^{-11}$	-109.9	$0.029 \cdot 10^{-11}$	0.12

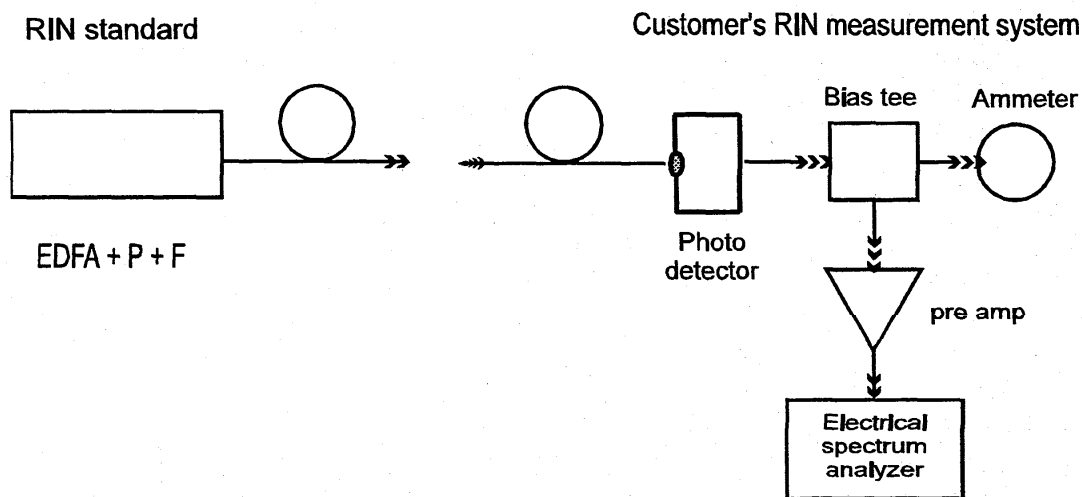


**Figure D1.** NIST RIN standard applied to customer's RIN measurement system.

### Application of the transfer standard to a RIN measurement system

When RIN is measured in the electrical domain, a bias tee sends the dc photocurrent from the photodetector to an ammeter while the ac noise is amplified, then displayed on a radio-frequency (rf) spectrum analyzer (Figure 1). The RIN is the noise power per unit bandwidth,  $\delta P_e(f)$ , weighted with the frequency-dependent calibration function  $\kappa(f)$  of the detection system (herein referred to as Kappa), and divided by the electrical dc power  $P_e$ . Thus

$$RIN = \frac{\kappa(f) \cdot \delta P_e(f)}{P_e} = \text{constant} , \quad (D.1)$$

where  $\delta P_e(f)$  is the noise after subtracting the thermal noise floor.

To calibrate a RIN measurement system, the customer connects the RIN standard using a quality FC/PC connector with standard single mode fiber. The  $\delta P_e(f)$  is measured on the rf spectrum analyzer; measure  $P_e(f)$  with a high accuracy voltmeter connected across a 50  $\Omega$  resistor. Substitute the value for the RIN of the standard to obtain Kappa. Solution of eq (1) for  $\kappa(f)$  gives

$$\kappa(f) = \frac{RIN \cdot P_e(f)}{\delta P_e(f)} . \quad (D.2)$$

To determine the RIN of an unknown source, the customer applies eq (2) with the values of Kappa obtained from the standard. Figure 2D is a sample graph of Kappa of the NIST RIN system using the standard.

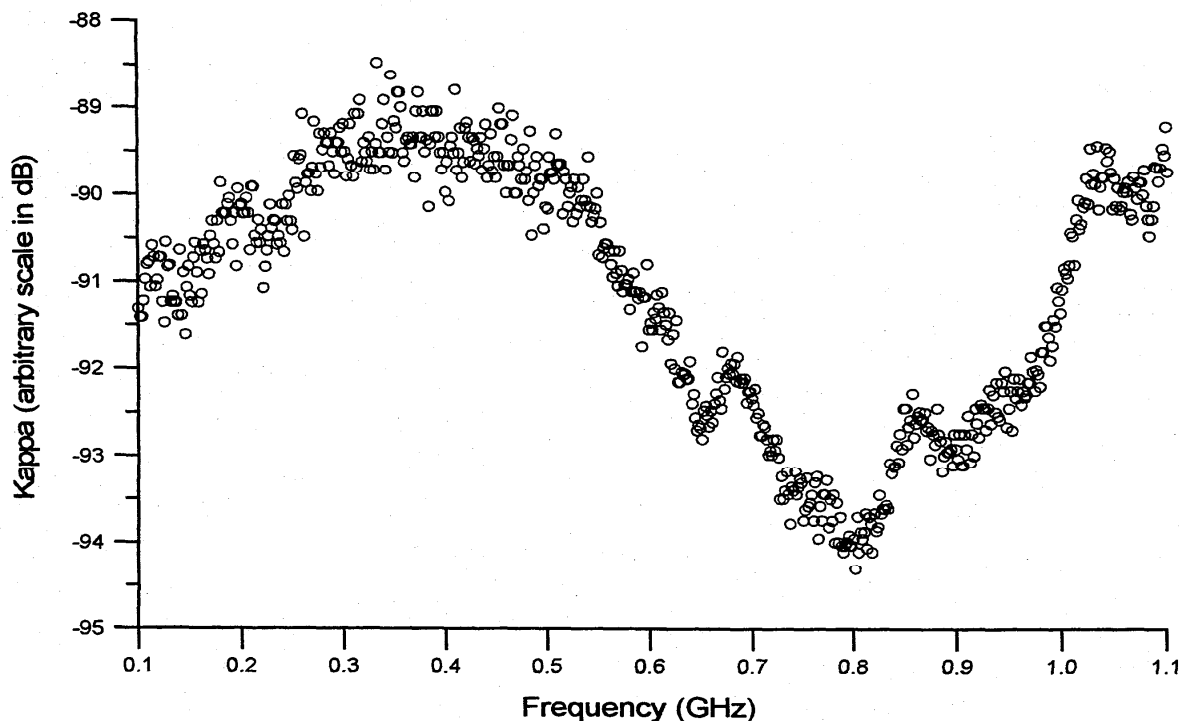


**Figure D2.** Graph of the frequency-dependent calibration function, Kappa, obtained for the NIST RIN measurement system by application of the RIN standard.

### Uncertainty Assessment

Estimates of uncertainty for the NIST RIN standard are determined from the repeatability error and the contributions of the optical spectrum analyzer parameters. All uncertainties related to the standard are TYPE A evaluations of standard uncertainty, in that each is obtained from measurements. There are no significant Type B errors [1].

The uncertainties are listed in Table D2. The RIN of the standard is the average of all RIN measurements used to calculate the repeatability error,  $U_{\text{REP}}$ . The uncertainties arising from the optical spectrum analyzer parameters are nonlinearity spectral responsivity  $U_{\text{LIN}}$ , wavelength distortion  $U_{\lambda}$ , and resolution bandwidth  $U_{\text{RBW}}$ .

**Table D2.** Summary of typical measurement uncertainties contributing to the total uncertainty in the RIN of the standard.

EDFA2 + F1	Uncertainty evaluation Type (A or B)	Standard uncertainty (1/Hz)	Standard uncertainty (dB/Hz)
$U_{REP}$	A	$0.000561 \cdot 10^{-11}$	0.002
$U_{LIN}$	A	$0.001180 \cdot 10^{-11}$	0.005
$U_{\lambda}$	A	$0.012315 \cdot 10^{-11}$	0.051
$U_{RBW}$	A	$0.000419 \cdot 10^{-11}$	0.002
<b>Expanded, U</b>	-	$0.029 \cdot 10^{-11}$	0.12
<b>Combined, <math>u_c</math></b>	-	$0.014475 \cdot 10^{-11}$	0.060

The repeatability error is calculated from the basic standard-deviation formula. The uncertainties for the OSA parameters are determined by application of the standard propagation of errors formula. The combined standard uncertainty  $u_c$  of the average RIN is determined by combining the Type A uncertainties ( $U_{REP}$ ,  $U_{LIN}$ ,  $U_{\lambda}$ ,  $U_{RBW}$ ) in quadrature. The expanded uncertainty, U, is twice the combined standard uncertainty. The values used to calculate the NIST expanded uncertainties appear in Table 2.

## Useful Information for Calibrating the User's Electrical Spectrum Analyzer for Scale Fidelity Correction

This section refers to Appendix A of the main document. Application of the RIN transfer standard to calibrate a RIN measurement system holds true for the rf electrical spectrum analyzer (ESA) set at a distinct group of function settings, such as sweep time, resolution and video bandwidth, internal attenuation, etc. Changing a function setting to accommodate a signal requires a new calibration, since the Kappa then obtained may differ slightly from the original. In addition, each ESA has a unique scale fidelity factor that accounts for the vertical position of the noise signal on the screen. RIN measurements for which the rf amplitude noise differs must be weighted with this factor, which like Kappa, is frequency dependent. The scale fidelity factor can be obtained using an rf signal generator, an attenuator, the ESA, and an rf power meter. Connector losses should be included and control settings kept the same as for a RIN measurement. The rf power is recorded at two different positions on the ESA with and without the attenuator. The scale fidelity correction for signals of varying magnitude can be expressed as a correction to Kappa at each frequency separately.

Below is an example of how we calibrate the NIST ESA. The attenuation of a 10 dB attenuator is measured as shown in the top part of Figure A.1 with the signal generator set at 600 MHz and power output at -50 dBm. Using the rf power meter the attenuation is measured to be 10.0 dB. With the signal generator set at 600 MHz and -70 dBm, the signal is positioned on the ESA screen as would occur for an actual noise measurement. The result is recorded with and without the attenuator. When our ESA is set at 5 dB per vertical division, the scale fidelity,  $S$ , is found to increase the difference between the two readings by 0.15 dB per division. Also, the manufacturer specifies that the amplitude error must be  $\leq 0.7$  dB over the ten divisions that compose the screen. If the difference between noise powers at different vertical positions on the screen is  $\delta P_1 - \delta P_2$  (at the same frequency), then the scale fidelity correction is

$$S_1 = \frac{\delta P_1}{\delta P_1 + 0.03 \cdot (\delta P_1 - \delta P_2)} \quad (\text{A.1})$$

Application of eq (A.1) to Kappa at each frequency (sections 9.1 and 9.2) gives



$$\kappa_{1,cor} = \frac{\kappa_{1,un} \cdot \delta P_1}{\delta P_1 - 0.03 \cdot (\delta P_1 - \delta P_2)}, \quad (A.2)$$

where the subscripts *cor* and *un* represent the corrected and uncorrected Kappas, respectively. This is a most general formula in which  $\delta P_1$  can be greater or less than  $\delta P_2$ . If it is greater, the corrected Kappa increases at the set calibration frequency. If it is less, the corrected Kappa decreases.

[1] B.N. Taylor and C.E. Kuyatt, "Guidelines for Evaluating and Expressing the Uncertainty of NIST Measurement Results, NIST Technical Note 1297, 1994 Edition.

For the Director,  
NIST

Report Prepared/Calibrated By:

---

Gordon Day, Chief  
Optoelectronics Division

---

Gregory E. Obarski  
Physicist  
Sources and Detectors Group

Folder No. and NIST ID: xx and yy  
Date of Report: March 1, 2000  
Reference: P.O. No. Mmm, 2/3/00

## Appendix E. Calibration Service

As appropriate, the customer may benefit more from a calibration service (CALSV) than a measurement assurance program (MAP). To use a CALSV, customers send their own devices to NIST for calibration instead of renting the NIST standard through the MAP. We refer to the customer's calibrated RIN device as a company standard. Although customers purchase their own components, NIST would be available for consultation on which components to purchase (but as a matter of policy does not recommend specific brands).

Calibration and traceability of the company standard to NIST would occur as a two step process. Periodically, perhaps once per year, the customer would send NIST his or her company standard for calibration. NIST calibrates the NIST RIN measurement system using the NIST standard, and then within a few minutes this calibrated system is used to calibrate the customer's RIN device. NIST will supply the customer with a calibration report, and make any recommendations needed for the customer to continue possessing a quality RIN standard. This procedure will increase the uncertainty in the RIN by about 0.03 dB over that of the MAP, which uses the NIST standard to calibrate the customer's RIN device directly. The increased uncertainty occurs because, in addition to the uncertainty in the NIST standard, the uncertainty inherent in the NIST RIN system is also transferred to the customer's company standard. However, if the RIN of the source can be approximated by thermal light, such as the NIST RIN standard, the combined uncertainty is reduced by determining the RIN from the same method used for the NIST RIN standard. In this method, the theory of the RIN of thermal light is applied to the optical power spectral density of the device as measured by the NIST optical spectrum analyzer, which is precisely calibrated as a standard. The latter method will be used at the customer's discretion.

**Appendix F: Sample Calibration Certificate**

**U.S. DEPARTMENT OF COMMERCE  
NATIONAL INSTITUTE OF STANDARDS AND TECHNOLOGY  
ELECTRONICS AND ELECTRICAL ENGINEERING LABORATORY  
Boulder, Colorado 80303**

**REPORT OF CALIBRATION BY NIST**

for

**Spectral Density of Relative Intensity Noise**

Submitted to:  
ABCDE Corp.  
Address

**Calibration Summary**

This report summarizes the measurement results for the spectral density of relative intensity noise (RIN) of the customer's noise source. The source is calibrated over the 0.1 GHz to 1.1 GHz frequency range. The measurements were performed in two steps. First, the NIST RIN measurement system was calibrated with the NIST RIN standard. Next, the RIN of the customer's device was measured with the calibrated RIN system. The NIST RIN standard is an erbium-doped fiber amplifier (EDFA) to which is coupled a linear polarizer (P) followed by a narrowband filter (F). Thus, it is represented by EDFA + P + F as shown in Figure F1. The EDFA has a built-in optical isolator to ensure that the amplified-spontaneous emission (ASE) that it emits is free from potential multiple interference effects such as ripple. High-quality FC/PC connectors and single-mode fiber are used throughout.

The RIN of the NIST standard was determined from measurements of its optical power spectral density (OPSD) as measured by a high resolution, grating-type, optical spectrum analyzer (OSA). The RIN is proportional to the autocorrelation of the measured OPSD, and is constant out to several tens of gigahertz. The uncertainties that contribute to the RIN are the repeatability in RIN

Folder No: bbbb

Date of Report: March 16, 2000

Reference: P.O. No. Tttt ee/yy/nm

**Table F1.** RIN of customer's device and uncertainty of RIN expressed in linear and logarithmic units.

Frequency range	RIN of customer's device		Expanded uncertainty	
	1/Hz	dB/Hz	1/Hz	dB/Hz
0.1-1 GHz	aaa	bbb	ccc	ddd

measurements as well as the uncertainties that arise from the OSA parameters involved in the measurement. Calibrations are performed after all equipment is warmed to steady-state thermal stability (several hours). The results of the RIN measurements on the customer's device are summarized in Table F1, where the expanded uncertainty reported is defined in the section on uncertainty assessment.

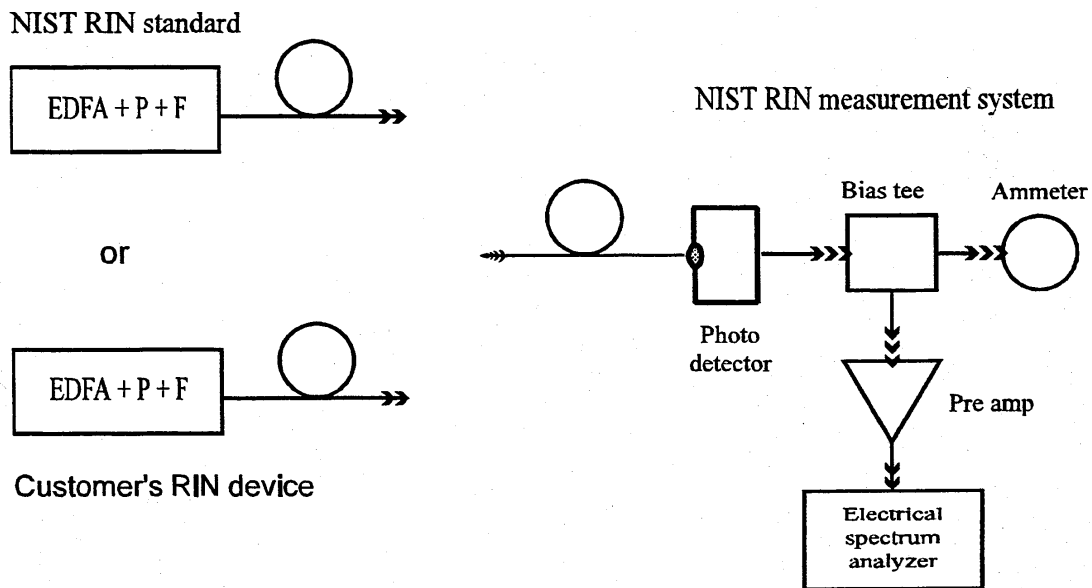


**Figure F1.** Calibration of the customer's RIN device using the NIST RIN measurement system as calibrated by the RIN standard

## Application of the transfer standard to a RIN measurement system

When the RIN of the customer's device is measured, we first calibrate the NIST RIN system with the NIST RIN standard. To measure RIN in the electrical domain, we use a bias tee to send the dc photocurrent to an ammeter, while the ac noise is amplified and displayed on a radio-frequency (rf) spectrum analyzer (Figure F1). The dc power is determined with a voltmeter connected across a 50  $\Omega$  resistor instead of the ammeter. If  $i$  is the current,  $v$  the voltage, and  $R$  the resistance, the dc power is  $P_e = Ri^2 = v^2/R$ . The RIN is the noise power per unit bandwidth,  $\delta P_e(f)$ , weighted with the frequency-dependent calibration function  $\kappa(f)$  of the detection system (herein referred to as Kappa), and divided by the electrical dc power  $P_e$ . Thus,

$$RIN = \frac{\kappa(f) \cdot \delta P_e(f)}{P_e} = \text{constant} , \quad (\text{F.1})$$

where  $\delta P_e(f)$  is the noise after subtracting the thermal noise floor.

To calibrate the NIST RIN measurement system we apply the RIN standard and measure  $\delta P_e(f)$  and  $P_e(f)$ . If  $R_s$  is the RIN of the standard, then from eq (F1) Kappa is

$$\kappa(f) = \frac{R_s \cdot P_e(f)}{\delta P_e(f)} . \quad (\text{F.2})$$

The RIN of an unknown source is determined by connecting the source to the NIST RIN measurement system and then measuring  $\delta P_e(f)$  and  $P_e(f)$ . By substituting Kappa into eq (F1), the RIN is

$$RIN_x(f) = \frac{P_e}{P_{ex}} \cdot \frac{\delta P_{ex}(f)}{\delta P_e(f)} \cdot R_s(f) . \quad (\text{F.3})$$

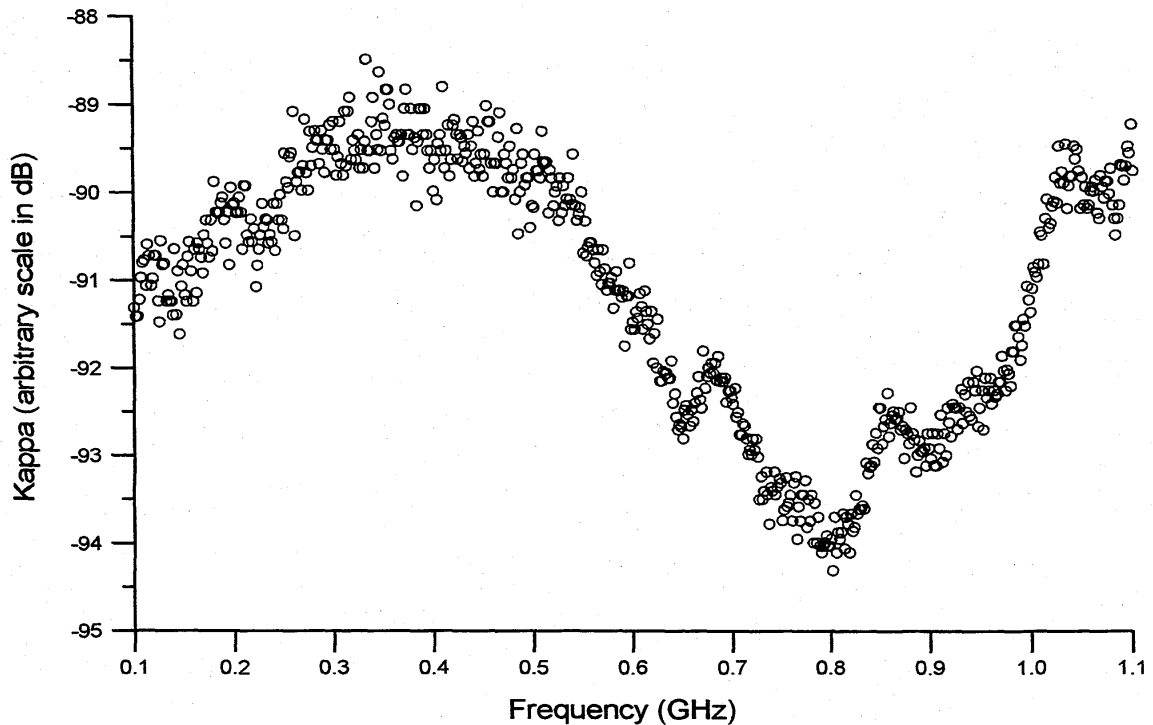


**Figure F2.** Graph of the frequency-dependent calibration function, Kappa, obtained for the NIST RIN measurement system by application of the RIN standard.

### Uncertainty Assessment

The uncertainty in calibrating the RIN of the customer's device will depend on whether it is a broadband source modelled after the NIST standard, or whether it is a laser. For a laser the total uncertainty is due to the NIST RIN standard plus the uncertainty contributed by the NIST RIN measurement system. The latter is the uncertainty in the calibration function (Kappa) and is determined at the time the calibration is performed. If the RIN of the source can be approximated by thermal light, such as the NIST RIN standard, however, the combined uncertainty is reduced by determining the RIN from the same method used for the NIST RIN standard. In this method the theory of the RIN of thermal light is applied to the optical power spectral density of the device as measured by the NIST optical spectrum analyzer, which has been accurately calibrated.

The uncertainty estimates for the NIST RIN standard are determined from the repeatability error

Folder No: bbbb

Date of Report: March 16, 2000

Reference: P.O. No. Tttt cc/yy/nn

**Table F2.** Summary of measurement uncertainties.

<b>EDFA2 + F1</b>	<b>Uncertainty evaluation Type (A or B)</b>	<b>Standard uncertainty (1/Hz)</b>	<b>Standard uncertainty (dB/Hz)</b>
$U_{REP}$	A	$0.000561 \cdot 10^{-11}$	0.002
$U_{LIN}$	A	$0.001180 \cdot 10^{-11}$	0.005
$U_{\lambda}$	A	$0.012315 \cdot 10^{-11}$	0.051
$U_{RBW}$	A	$0.000419 \cdot 10^{-11}$	0.002
<b>Combined, <math>u_c</math></b>	-	$0.014475 \cdot 10^{-11}$	0.06
<b>Expanded, U</b>	-	$0.029 \cdot 10^{-11}$	0.12

and the contributions of the optical spectrum analyzer parameters. All uncertainties related to the standard are TYPE A evaluations of standard uncertainty, in that each is obtained from measurements. There are no significant Type B errors [1].

The uncertainties are listed in Table F2. The RIN of the standard is the average of all RIN measurements used to calculate the repeatability error,  $U_{REP}$ . The uncertainties arising from the optical spectrum analyzer parameters are nonlinearity spectral responsivity  $U_{LIN}$ , wavelength distortion  $U_{\lambda}$ , and resolution bandwidth  $U_{RBW}$ .

The repeatability error is calculated from the basic standard-deviation formula. The uncertainties for the OSA parameters are determined by application of the standard propagation of errors formula. The combined standard uncertainty  $u_c$  of the average RIN is determined by combining the Type A uncertainties ( $U_{REP}$ ,  $U_{LIN}$ ,  $U_{\lambda}$ ,  $U_{RBW}$ ) in quadrature. The expanded uncertainty, U, is twice the combined standard uncertainty. The values used to calculate the NIST expanded uncertainties are listed in Table F2.

## Useful Information for Calibrating the User's Electrical Spectrum Analyzer for Scale Fidelity Correction

This section refers to Appendix A of the main document. Application of the RIN transfer standard to calibrate a RIN measurement system holds true for the rf electrical spectrum analyzer (ESA) set at a distinct group of function settings, such as sweep time, resolution and video bandwidth, internal attenuation, etc. Changing a function setting to accommodate a signal requires a new calibration, since the Kappa then obtained may differ slightly from the original. In addition, each ESA has a unique scale fidelity factor that accounts for the vertical position of the noise signal on the screen. RIN measurements for which the rf amplitude noise differs must be weighted with this factor, which like Kappa, is frequency dependent. The scale fidelity factor can be obtained using an rf signal generator, an attenuator, the ESA, and an rf power meter. Connector losses should be included and control settings kept the same as for a RIN measurement. The rf power is recorded at two different positions on the ESA with and without the attenuator. The scale fidelity correction for signals of varying magnitude can be expressed as a correction to Kappa at each frequency separately.

Below is an example of how we calibrate the NIST ESA. The attenuation of a 10 dB attenuator is measured as shown in part "a" of Figure A.1 with the signal generator set at 600 MHz and power output at -50 dBm. Using the rf power meter, the attenuation is measured to be 10.0 dB. With the signal generator set at 600 MHz and -70 dBm, the signal is positioned on the ESA screen as would occur for an actual noise measurement. The result is recorded with and without the attenuator. When our ESA is set at 5 dB per vertical division, the scale fidelity, S, is found to increase the difference between the two readings by 0.15 dB per division. Also, the manufacturer specifies that the amplitude error must be  $\leq 0.7$  dB over the 10 divisions that compose the screen.

If the difference between noise powers at different vertical positions on the screen is  $\delta P_1 - \delta P_2$  (at the same frequency), then the scale fidelity correction is

$$S_1 = \frac{\delta P_1}{\delta P_1 + 0.03 \cdot (\delta P_1 - \delta P_2)}, \quad (\text{A.1})$$



Application of eq (A.1) to Kappa at each frequency (sections 9.1, 9.2) gives

$$\kappa_{1,cor} = \frac{\kappa_{1,un} \cdot \delta P_1}{\delta P_1 + 0.03 \cdot (\delta P_1 - \delta P_2)}, \quad (A.2)$$

where the subscripts *cor* and *un* represent the corrected and uncorrected Kappas, respectively. This is a most general formula, in which  $\delta P_1$  can be either greater or less than  $\delta P_2$ . If it is greater, the corrected Kappa increases at the set calibration frequency. If it is less, the corrected Kappa decreases.

[1] B.N. Taylor and C.E. Kuyatt, "Guidelines for Evaluating and Expressing the Uncertainty of NIST Measurement Results, NIST Technical Note 1297, 1994 Edition.

For the Director,  
NIST

Report Prepared/Calibrated By:

---

G. W. Day, Chief  
Optoelectronics Division

---

Gregory E. Obarski  
Physicist  
Sources and Detectors Group

Folder No: bbbb  
Date of Report: March 16, 2000  
Reference: P.O. No. Tttt ee/yy/nm

## **Appendix G: Shipping Instructions**

The instrument to be shipped should be placed in a padded box with sufficient foam to protect it from mechanical shock, vibration, and other environmental hazards. The operating manual for the optical fiber amplifier should be included, as well as specifications for the filter and polarizer. If appropriate, the customer should specify the operating value of the pump current for the EDFA if it is adjustable. All cables and connectors needed to calibrate the equipment should be included. All parts belonging to the instrument will be returned by NIST.

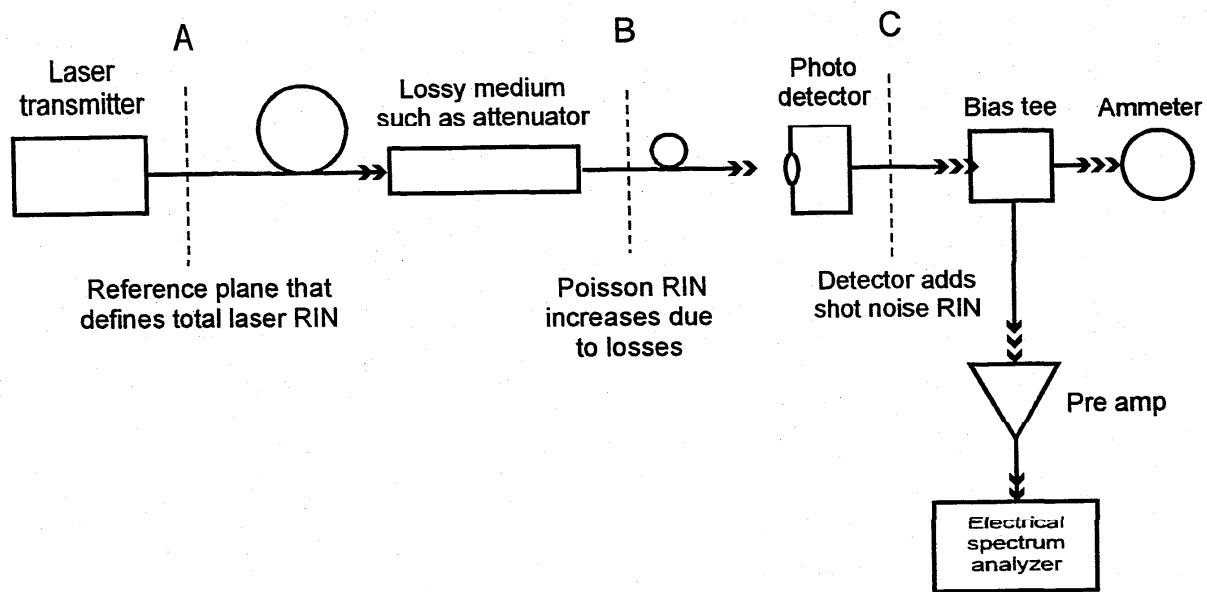


Figure 2.3.1 Basic RIN measurement system.

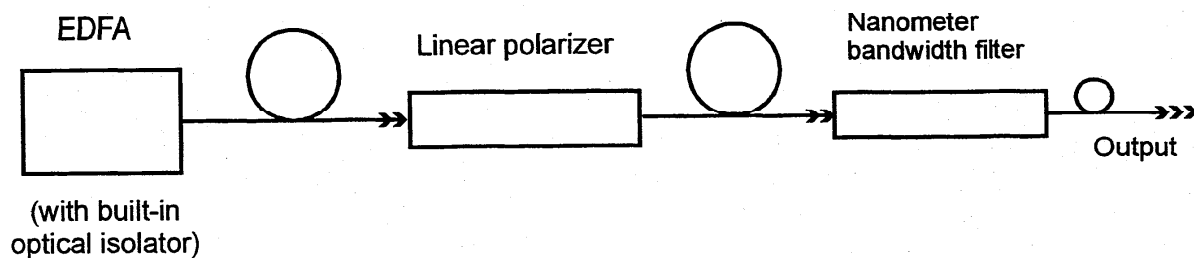


Figure 3.1.1. Form of the RIN standard.

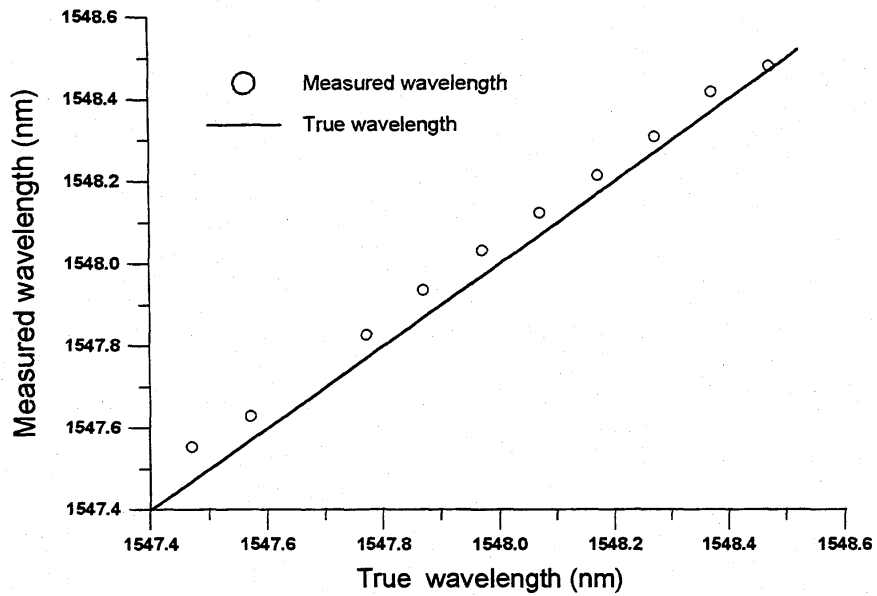


Figure 5.2.1. Comparison of wavelengths measured by the OSA with the true wavelength in the 1548 nm region.

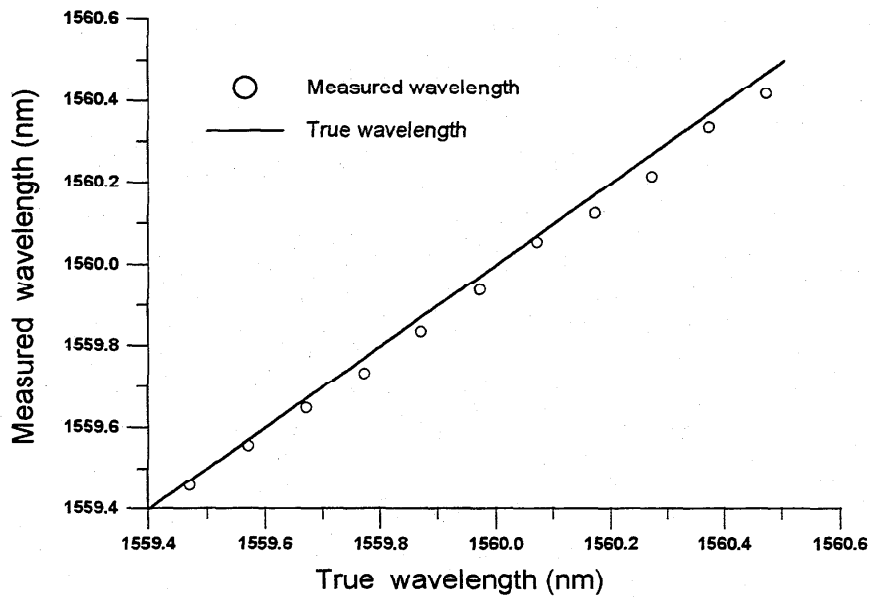
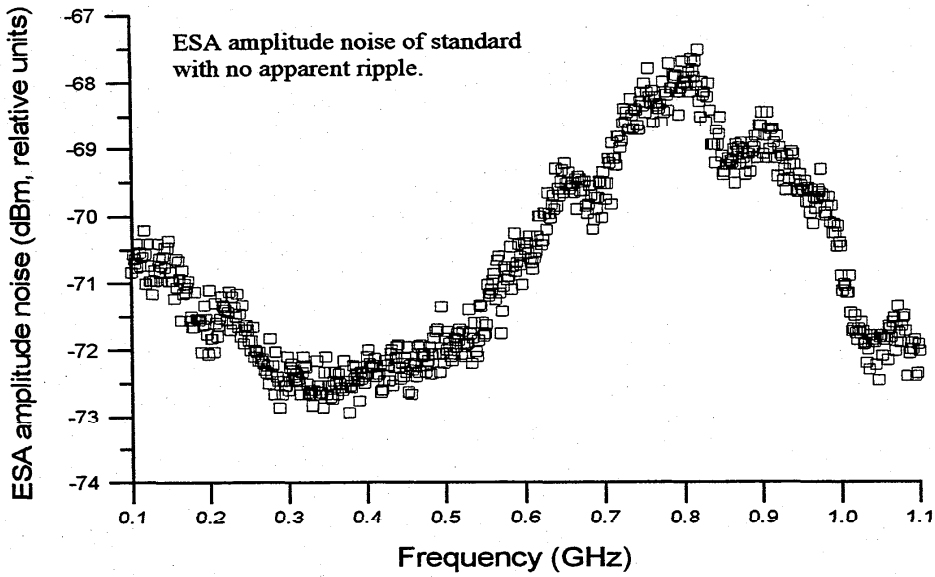


Figure 5.2.2. Comparison of wavelengths measured by the OSA with the true wavelength in the 1560 nm region.



Figures 6.2.1. Absence of ripple on the rf noise from the RIN standard over the frequency band of 0.1 GHz through 1.1 GHz.

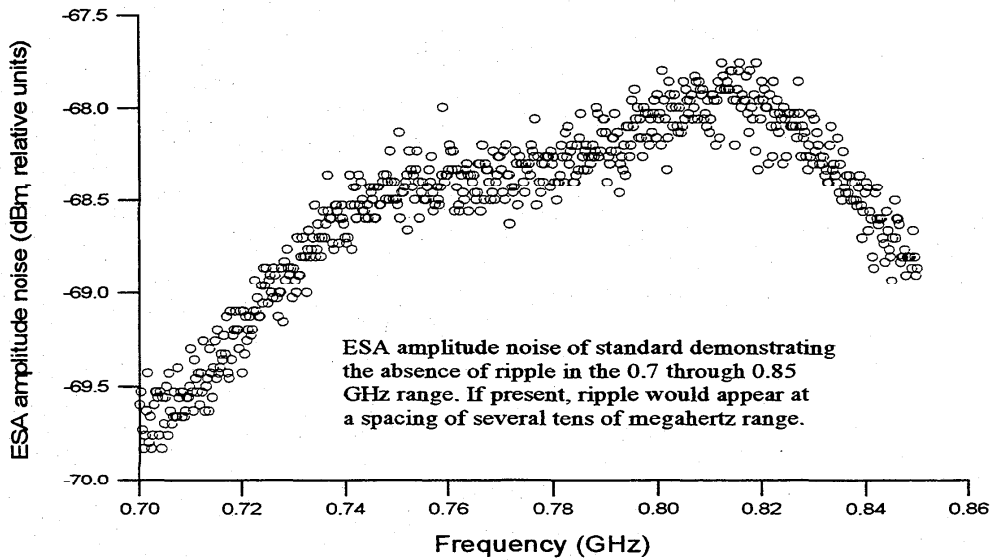


Figure 6.2.2. Absence of ripple on the rf noise from the RIN standard over the frequency band of 0.7 GHz through 0.85 GHz.

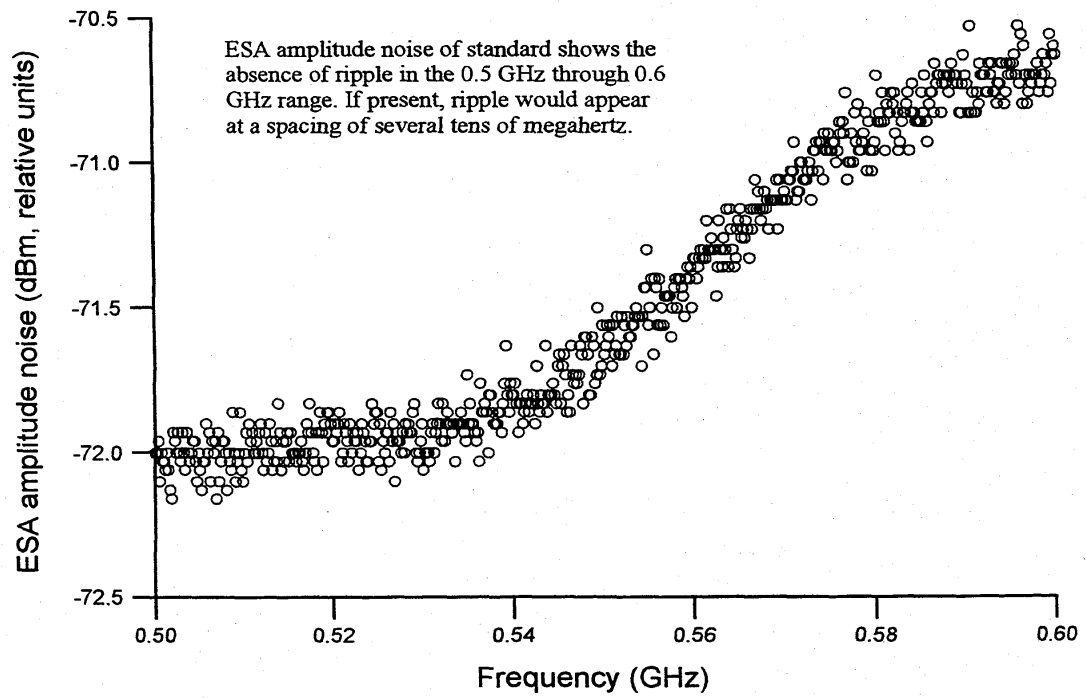


Figure 6.2.3. Absence of ripple on the rf noise from the RIN standard over the frequency bands of 0.5 GHz through 0.6 GHz.

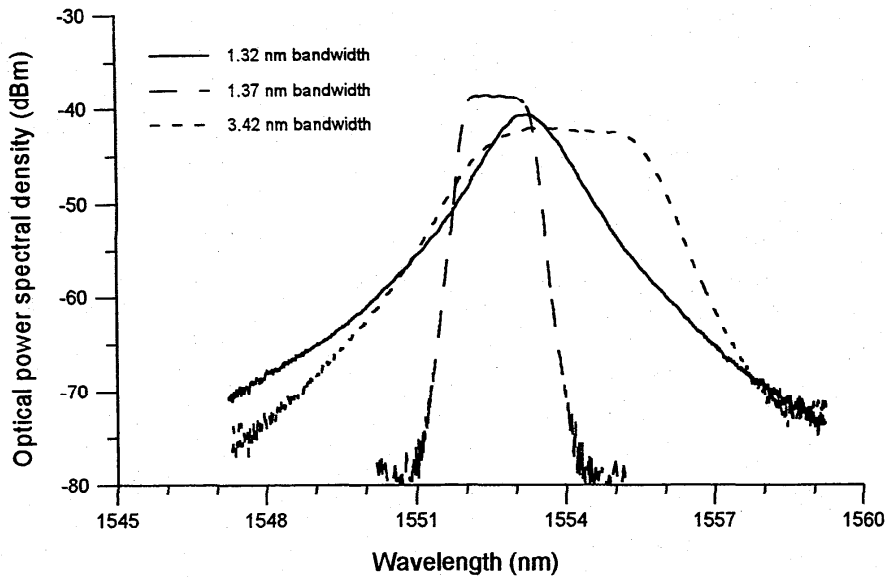


Figure 6.4.1. Optical power spectral density of the three filters F1, F2, and F3 used in this study.

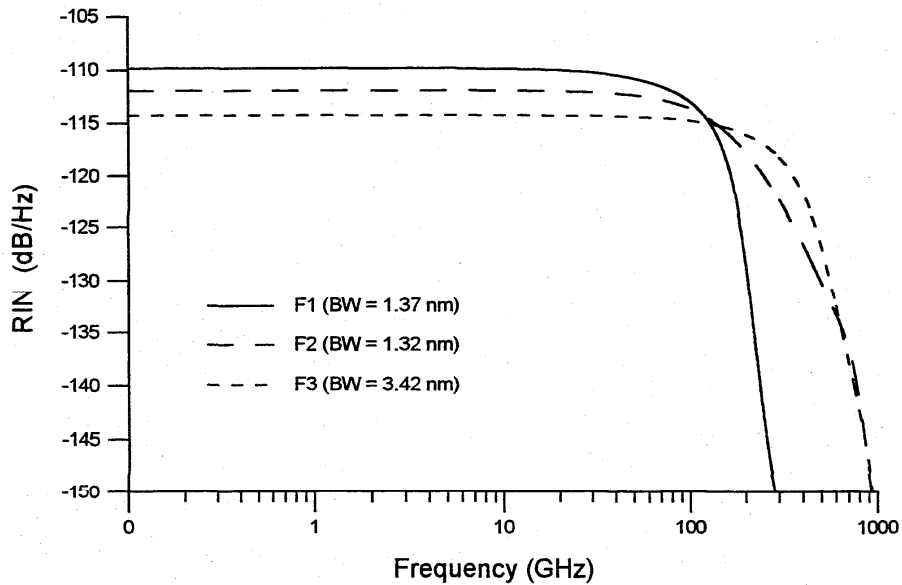


Figure 6.4.2. RIN of F1, F2, and F3 from near zero to 1000 GHz using EDFA2.

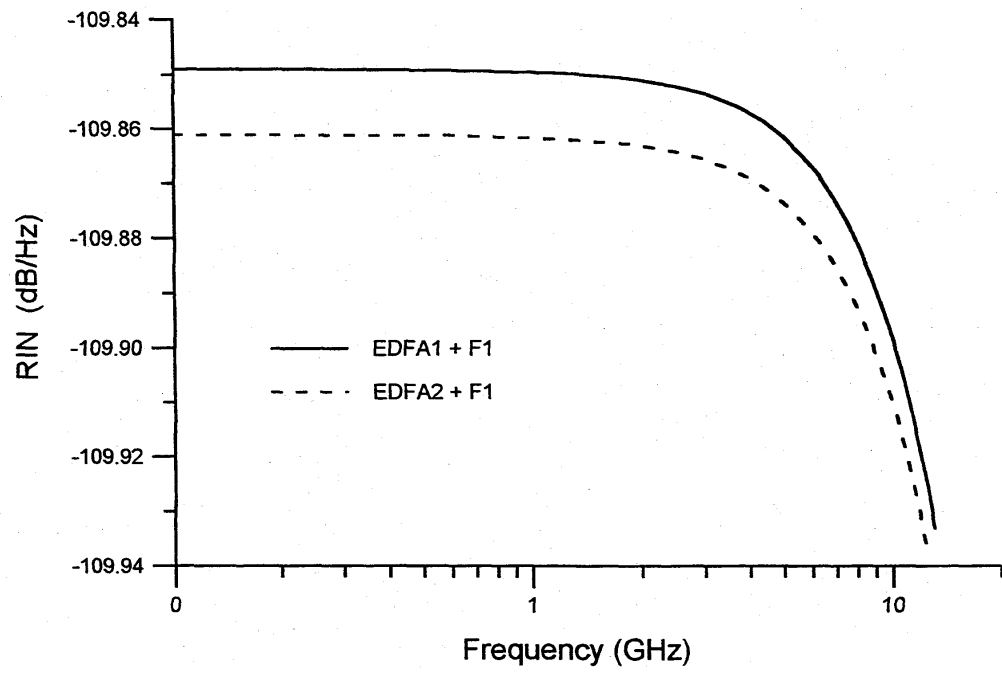


Figure 6.4.3. Comparison of the RIN from F1 using EDFA1 and EDFA2.



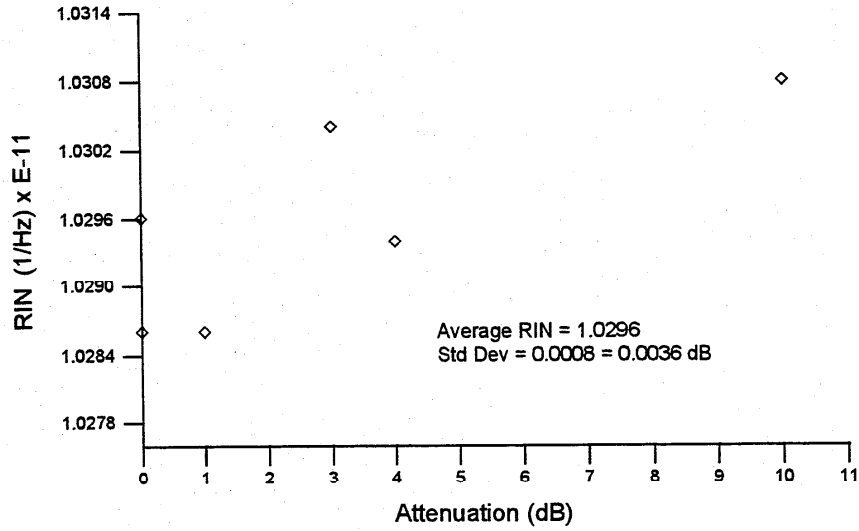


Figure 6.6.1. RIN of EDFA1 + F1 vs. attenuation. Any apparent trend is of no practical significance.

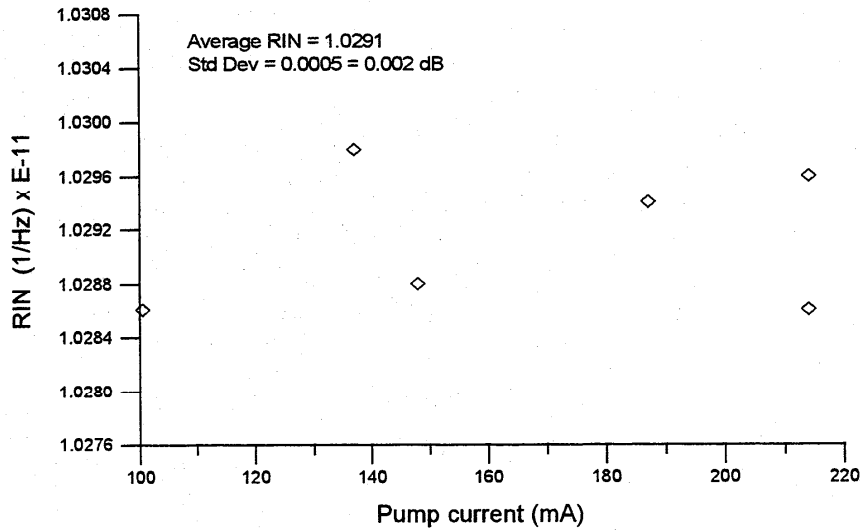


Figure 6.6.2. RIN of EDFA1 + F1 vs. pump current of the EDFA.

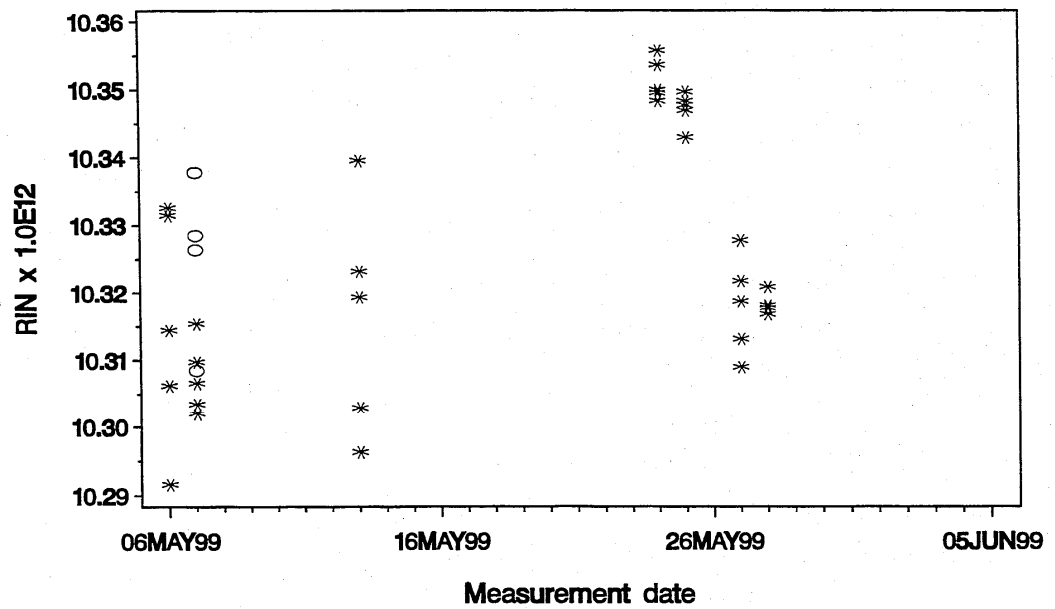


Figure 7.1.1. RIN of the standard over a three-week period. Circles represent second set of five measurements taken on May 5, 1999.

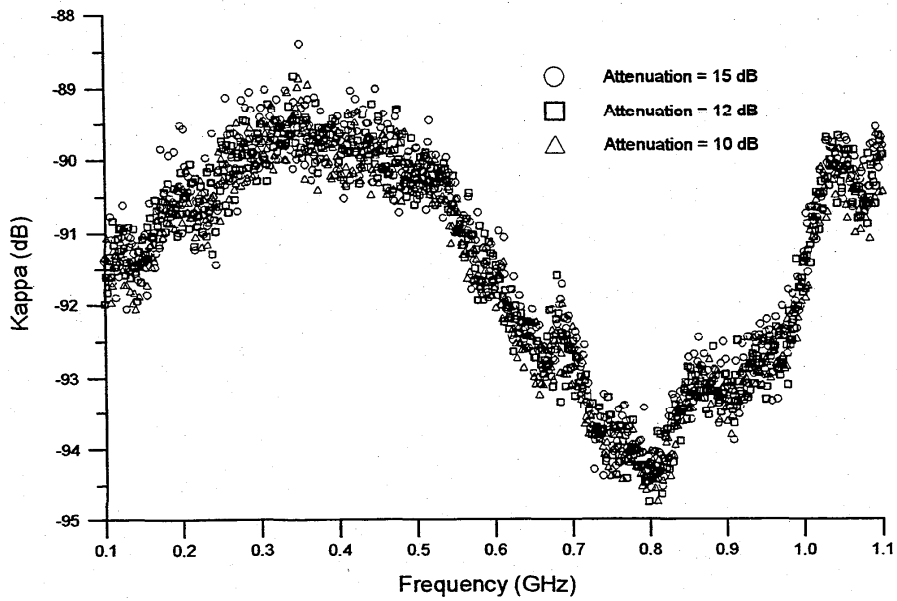


Figure 8.1.1. Calibration function of the laser versus frequency for various attenuation levels.

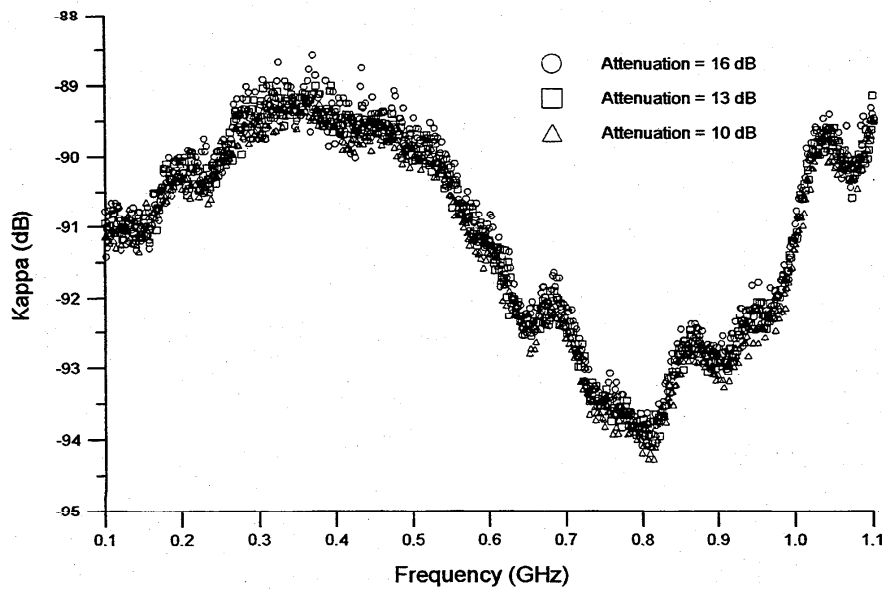


Figure 8.1.2. Calibration function of the laser versus frequency for similar but different attenuation levels.

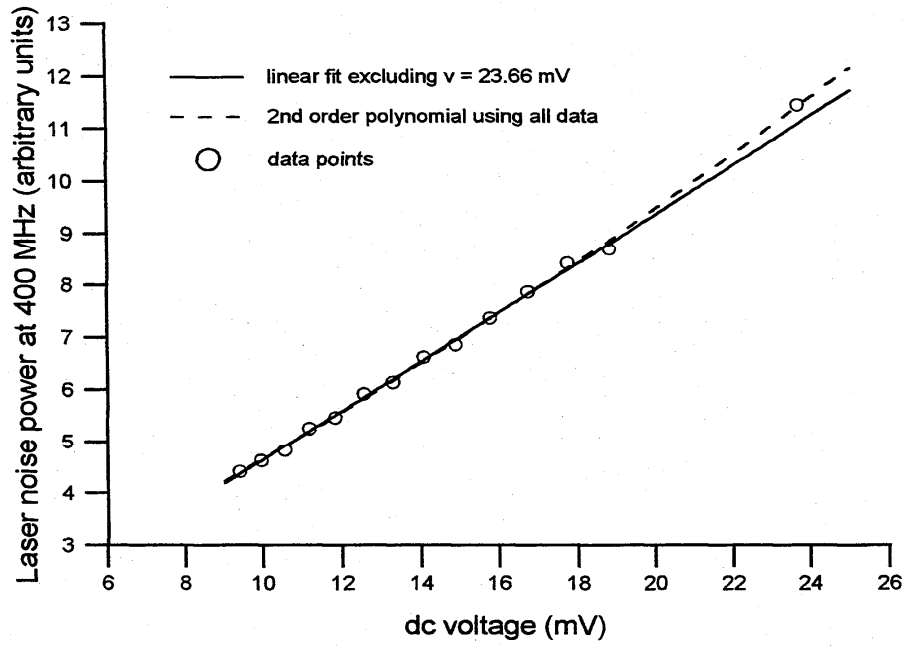


Figure 8.1.3. Electrical noise power of laser at 400 MHz versus dc voltage.

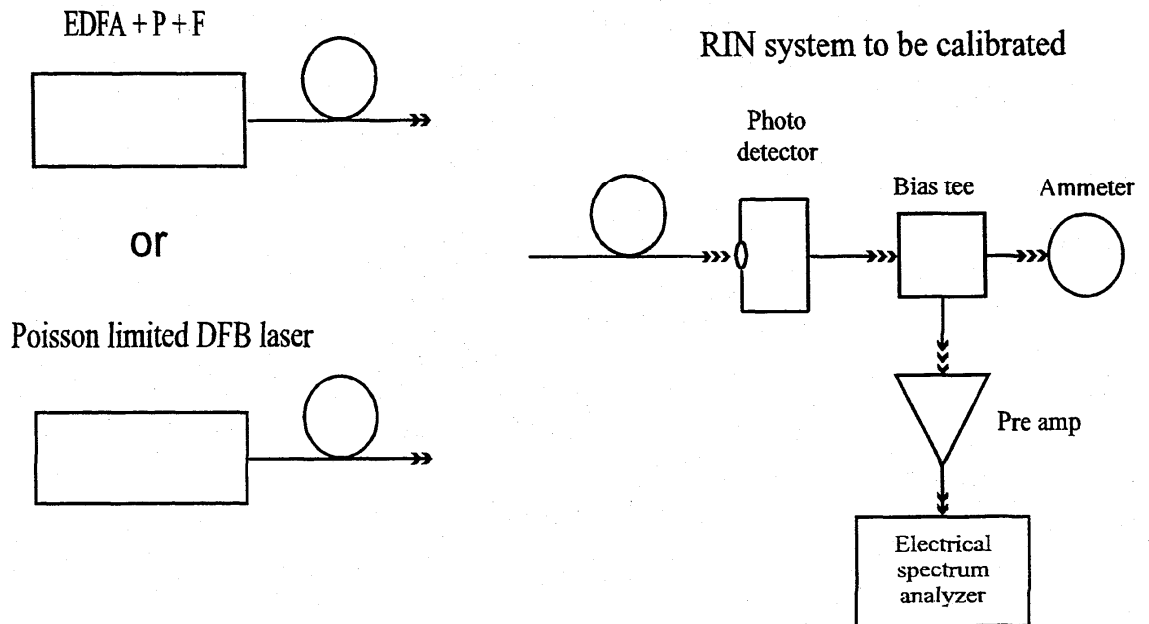


Figure 9.1. Calibration of the RIN system using the standard and the laser.

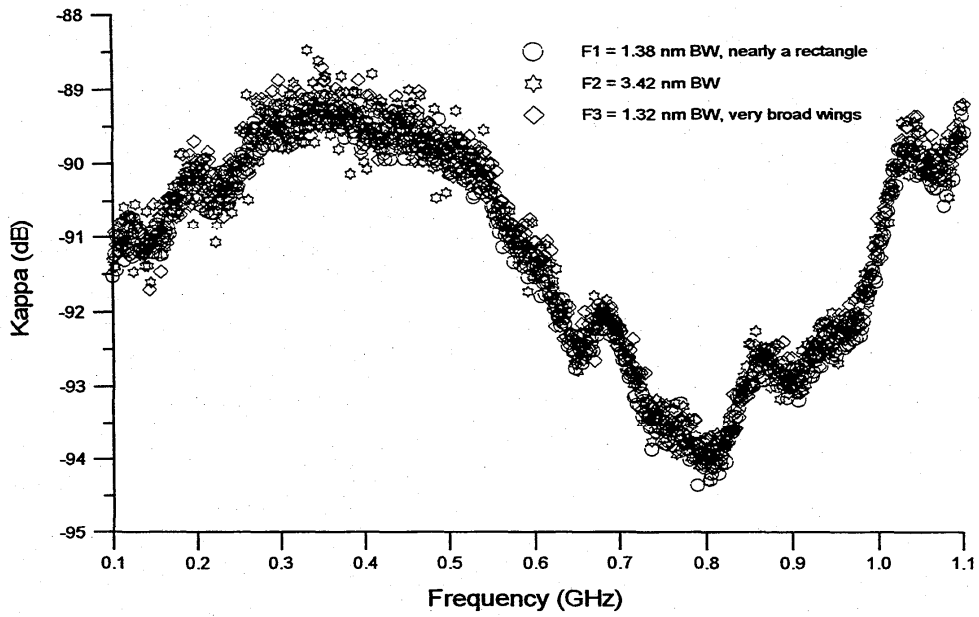


Figure 10.1.1. Comparison of Kappas using EDFA2 with filters F1, F2, or F3.

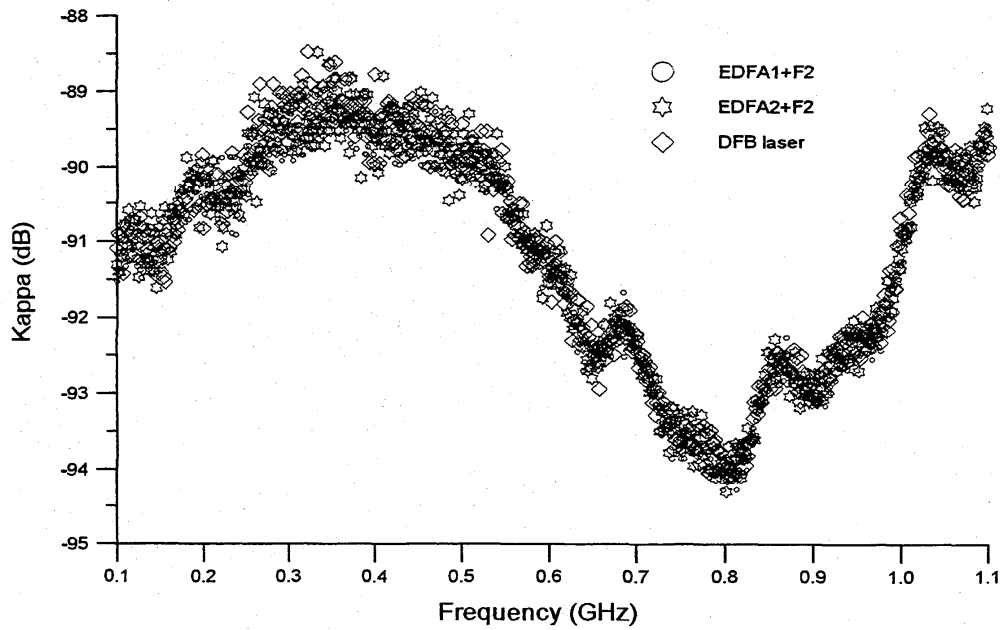


Figure 10.1.2. Comparison of Kappas from two different EDFAs + F2 with the laser.

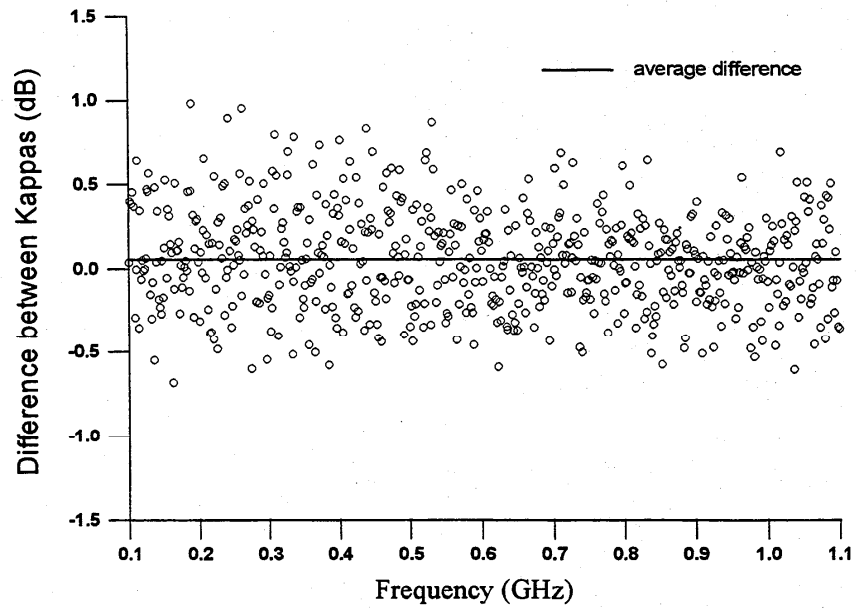


Figure 10.1.3 . Difference between Kappas from the laser and EDFA1 + F2. The data range from -1 to +1 dB. The average difference is 0.056 dB.

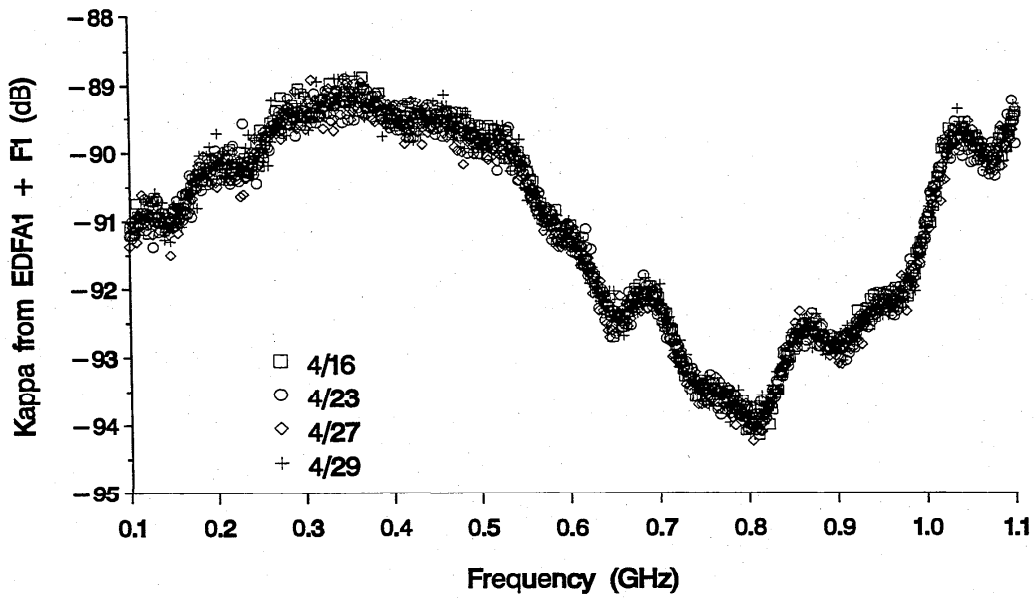


Figure 10.3.1. Kappa determined on four different days from EDFA1 + F1.

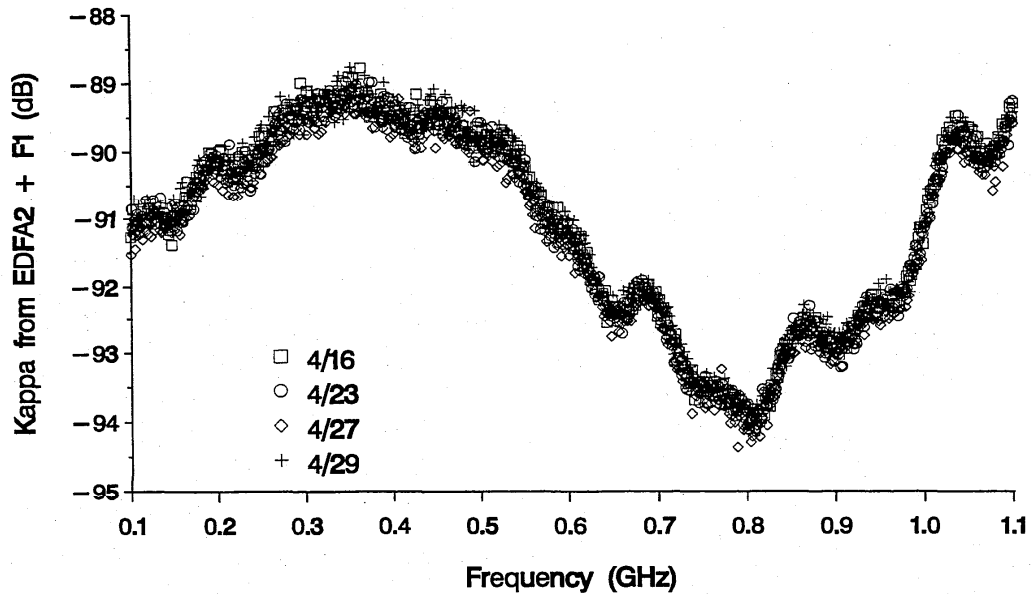


Figure 10.3.2. Kappa determined on four different days from EDFA2 + F1.

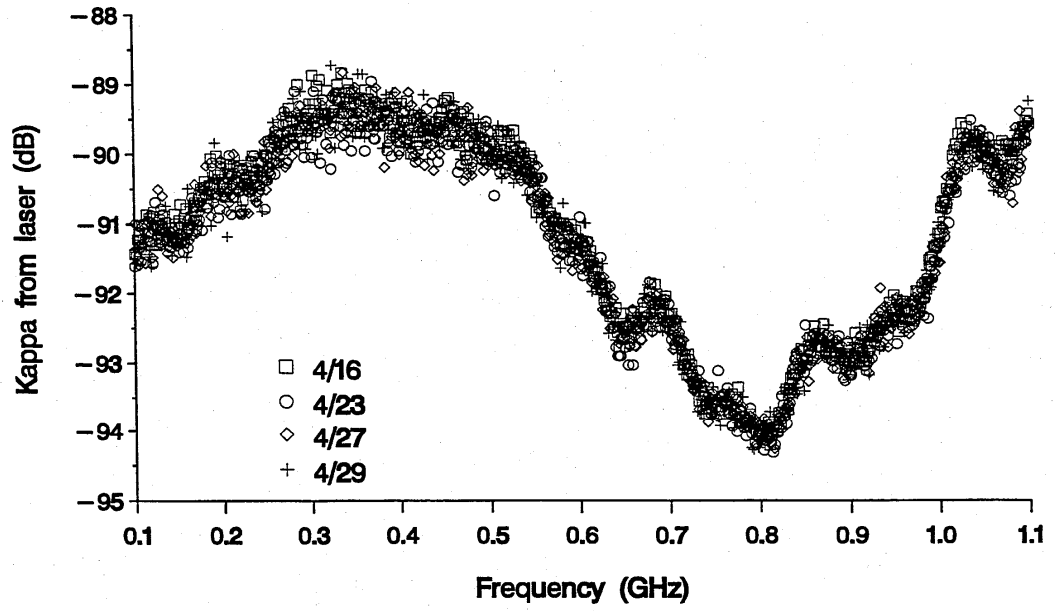


Figure 10.3.3. Kappa determined on four different days from the laser.



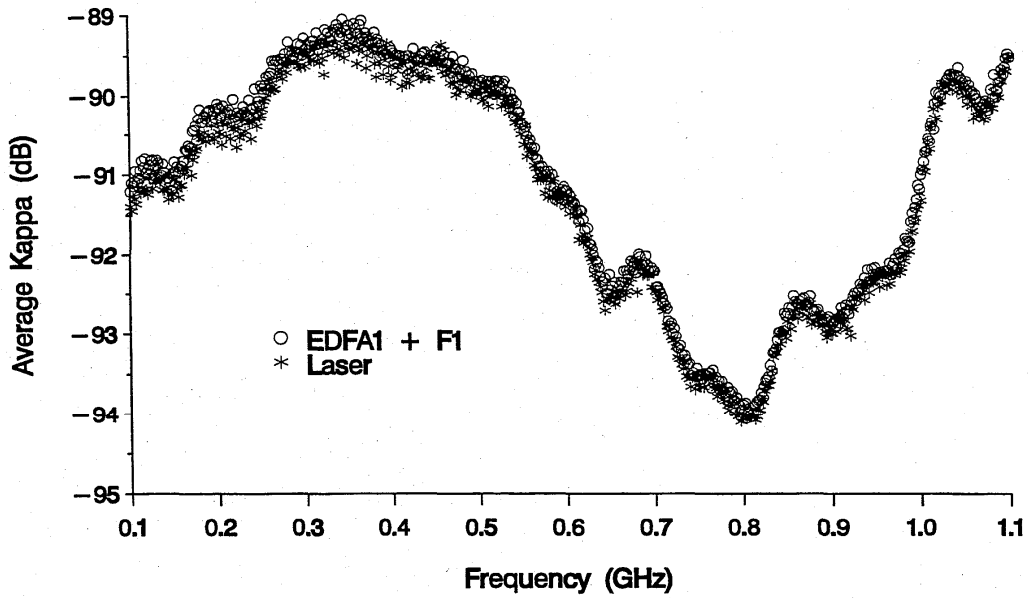


Figure 10.3.4. Comparison of Kappa from EDFA1 + F1 and the laser. Data were averaged over the four days shown in Figures 10.3.1 (EDFA1 + F1) and 10.3.3 (laser).

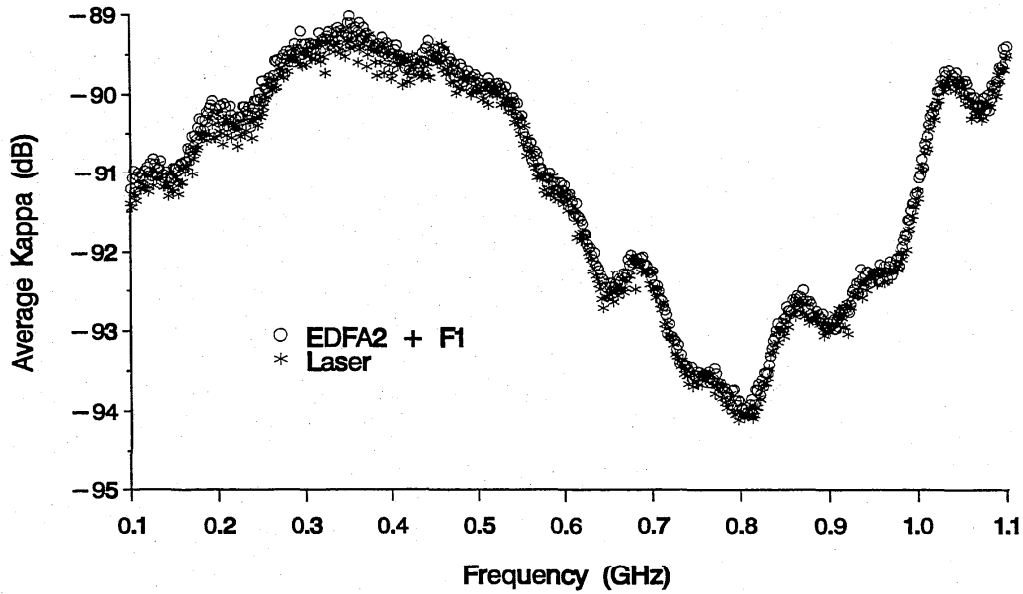


Figure 10.3.5. Comparison of Kappa from EDFA2 + F1 and the laser. Data were averaged over the four days shown in Figures 10.3.2 (EDFA2 + F1) and 10.3.3 (laser).

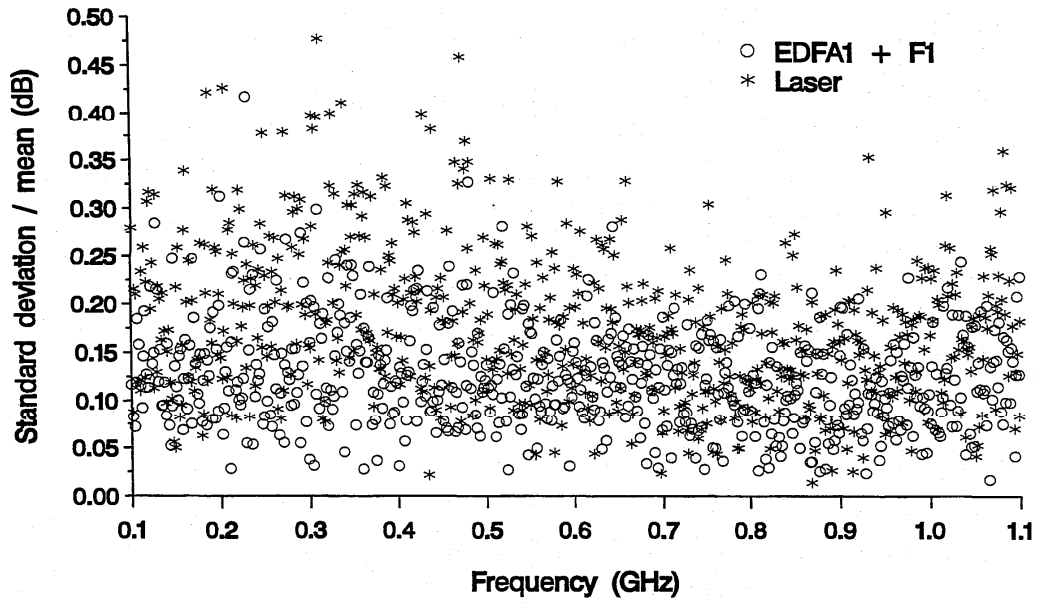


Figure 10.3.6. Comparison of the frequency dependence of the normalized standard deviation of the four data sets for Kappa from EDFA1 + F1 (Kappa values shown in Figure 10.3.1) and the corresponding four data sets from the laser (Kappa values shown in Figure 10.3.3).

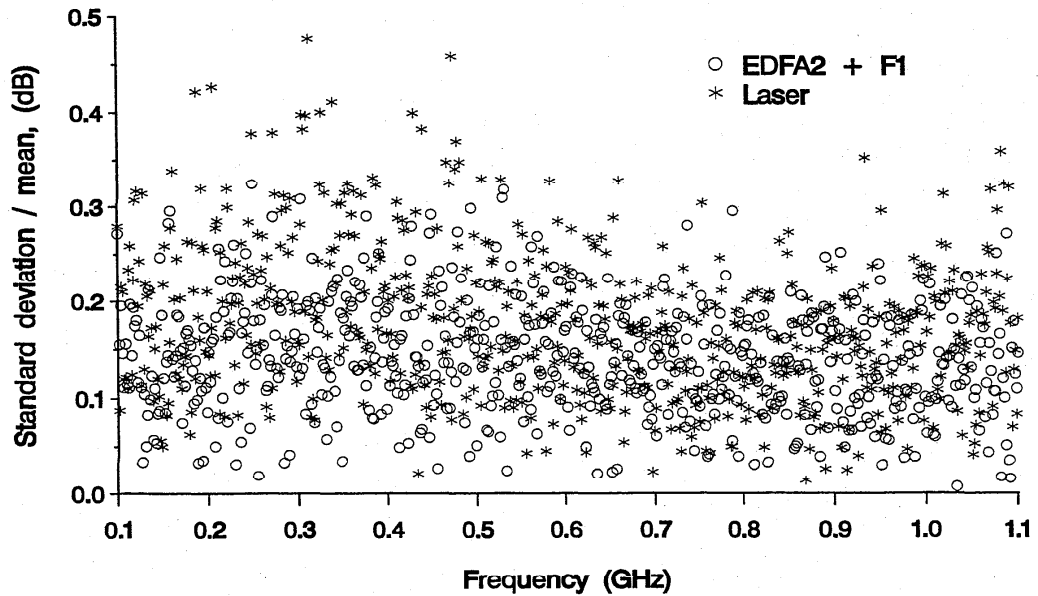


Figure 10.3.7. Comparison of the frequency dependence of the normalized standard deviation of the four data sets for Kappa from EDFA2 + F1 (Kappa values shown in Figure 10.3.2) and the corresponding four data sets from the laser (Kappa values shown in Figure 10.3.3).

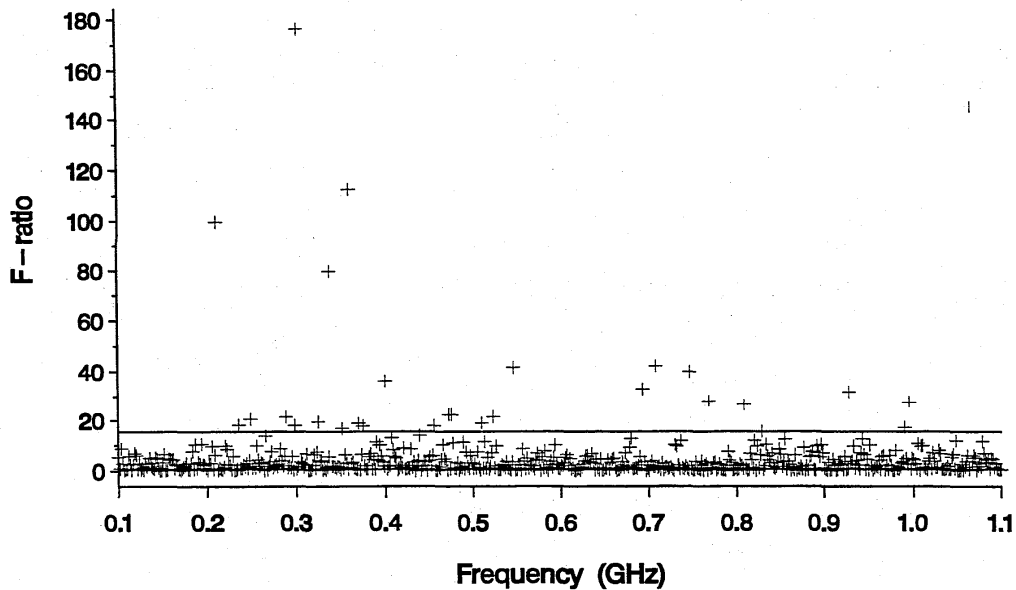


Figure 10.4.1. F-ratio versus frequency. The F-ratio shown is the variance of each Kappa from the laser divided by the variance of the Kappa from the EDFA1 + F1 at each frequency. The two reference lines represent the critical values for the F-test at the 0.05 level of significance.

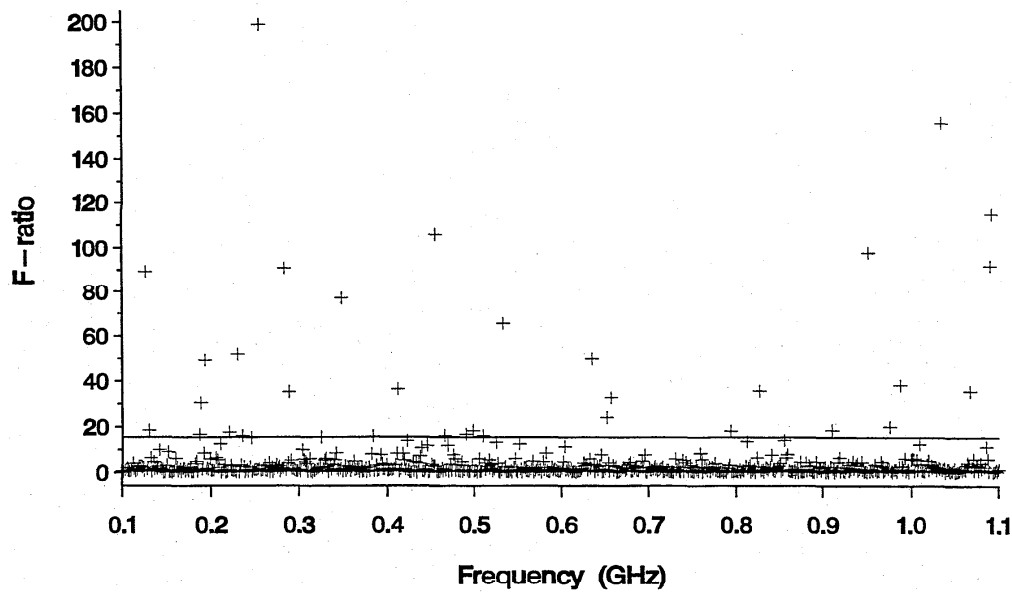


Figure 10.4.2. F-ratio versus frequency. The F-ratio shown is the variance of each Kappa from the laser divided by the variance of the Kappa from the EDFA2 + F1 at each frequency. The two reference lines represent the critical values for the F-test at the 0.05 level of significance. An F-ratio of 428.863 at 1.08 GHz is not shown.

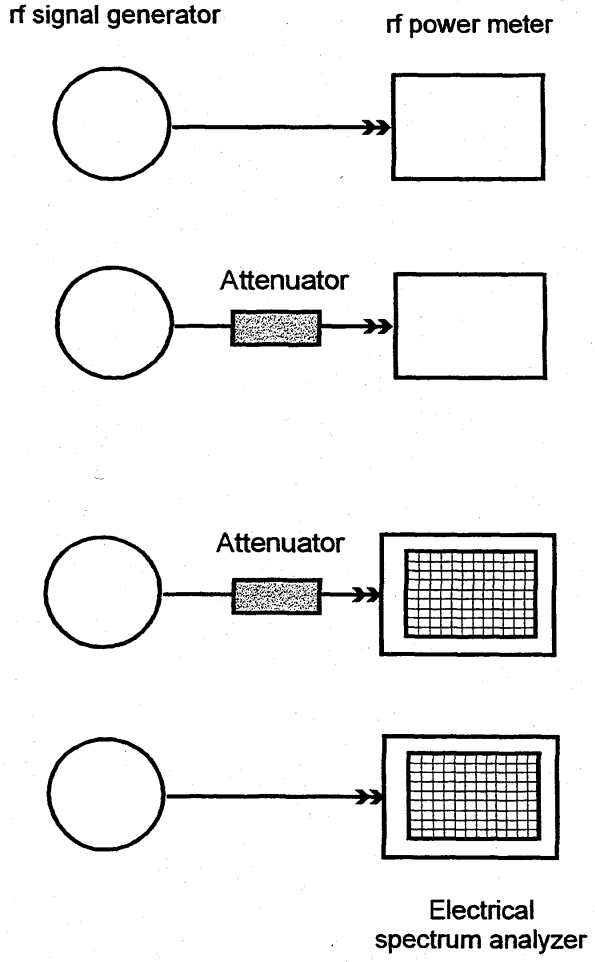


Figure A1. Measurement of the scale fidelity of the electrical spectrum analyzer using rf signal generator and attenuator, with output power traceable to rf power meter.

## THE SP 250 SERIES ON NIST MEASUREMENT SERVICES\*

SP 250-1	Spectral Radiance Calibrations PB87179883	SP 250-24	Standard Cell Calibrations PB88123690
SP 250-2	Far Ultraviolet Detector Standards PB87227609	SP 250-25	Calibration Service for Inductive Voltage Dividers
SP 250-3	Radiometric Standards in the Vacuum Ultraviolet PB87227625	SP 250-26	NBS Phase Angle Calibration Services PB88225636
SP 250-4	Fricke Dosimetry in High-Energy Electron Beams PB88110374	SP 250-27	AC-DC Difference Calibrations PB892222616
SP 250-5	Alpha-Particle Calibrations PB88168620	SP 250-28	Solid-State DC Voltage Standard Calibrations PB88168703
SP 250-6	Regular Spectral Transmittance PB88108550	SP 250-29	Traceable Frequency Calibrations PB88168364
SP 250-7	Radiance Temperature Calibrations PB88123674	SP 250-30	GOES Satellite Time Code Dissemination: Description and Operation PB88168760
SP 250-8	Spectral Reflectance PB88109905	SP 250-31	Mass Calibrations PB89153894
SP 250-9	Calibration of Beta-Particle-Emitting Ophthalmic Applicators PB88108535	SP 250-32	A Calibration Service for 30 MHz Attenuation and Phase Shift PB88238324
SP 250-10	Radioactivity Calibrations with the "4 $\pi$ " Gamma Ionization Chamber and Other Radioactivity Calibration Capabilities PB88123708	SP 250-33	A Calibration Service for Voltage Transformers and High-Voltage Capacitors PB882252903
SP 250-11	Dosimetry for High Dose Applications PB88201587	SP 250-34	High Vacuum Standard and Its Use PB89193841
SP 250-12	Neutron Personnel Dosimetry PB87227617	SP 250-35	The Calibration of Thermocouples and Thermocouple Materials PB89209340
SP 250-13	Activation Foil Irradiation with Californium Fission Sources PB88217443	SP 250-36	A Calibration Service for Current Transformers PB91216770
SP 250-14	Activation Foil Irradiation by Reactor Cavity Fission Sources PB88217435	SP 250-37	Photometric Calibrations PB97148472
SP 250-15	Photometric Calibrations PB88153747	SP 250-38	NIST Leak Calibration Service PB92149772
SP 250-16	Calibration of X-Ray and Gamma-Ray Measuring Instruments PB88211826	SP 250-39	NIST Pressure Calibration Service PB94164043
SP 250-17	The NBS Photodetector Spectral Response Calibration Transfer Program PB88201595	SP 250-40	Absorbed-Dose Calibration of Ionization Chambers in a <sup>60</sup> Co Gamma-Ray Beam <b>No PB number</b>
SP 250-18	Neutron Source Strength Calibrations PB88211818	SP 250-41	Spectroradiometric Detector Measurements: Part I - Ultraviolet Detectors and Part II - Visible to Near-Infrared Detectors PB98-149073
SP 250-19	Calibration of Gamma-Ray-Emitting Brachytherapy Sources PB89193858	SP 250-42	Spectroradiometric Detector Measurements: Part III - Infrared Detectors PB99-134371
SP 250-20	Spectral Irradiance Calibrations PB88123781	SP 250-43	Radiance Temperature Calibrations PB98-141047
SP 250-21	Calibration of Beta-Particle Radiation Instrumentation PB88201579	SP 250-44	Radiation Processing Dosimetry Calibration Services and Measurement Assurance Program PB98-140973
SP 250-22	Platinum Resistance Thermometer Calibrations PB88138367		
SP 250-23	Liquid-in-Glass Thermometer Calibration Service PB89128888		

\* Entries containing a stock number (SN003-003-) can be purchased from the Superintendent of Documents, U.S. Government Printing Office, Washington, DC 20402-9325. GPO will accept checks, money orders, VISA, and MasterCard. For more information, or to place an order, call (202) 512-1800. Be sure to cite the stock number on all orders.

Entries containing PB numbers can be purchased from the National Technical Information Service, Springfield, VA 22161. NTIS will accept American Express in addition to the payment methods listed for GPO. For more information or to place an order call (800) 553-6487. Fax: (703) 321-8547. Be sure to cite the PB number on all orders.

Entries without stock or PB numbers are in preparation.

## THE SP 250 SERIES ON NIST MEASUREMENT SERVICES\* — Continued

- SP 250-45 Radiation Processing Dosimetry Calibration Services: Manual of Calibration Procedures  
PB98-140981
- SP 250-46 NIST Multifunction Calibration System  
PB98-131279
- SP 250-47 NIST Calibration Service for Capacitance Standards at Low Frequencies  
PB98-144687
- SP 250-48 Spectral Reflectance  
PB98-149016
- SP 250-49 NIST Calibration Services for Gas Flow Meters: Piston Prover and Bell Prover  
Gas Flow Facilities  
PB99-107260
- SP 250-51 Calibration Service of Optoelectronic Frequency Response at 1319 nm for Combined Photodiode/rt Power Sensor Transfer Standards  
SN003-003-03623-4, PB2000-103300
- SP 250-52 Error Analysis and Calibration Uncertainty of Capacitance Standards at NIST  
SN003-003-03633-1, PB2000-103674
- SP 250-53 Calibration Service for Spectral Responsivity of Laser and Optical-Fiber Power Meters at Wavelengths Between 0.4  $\mu\text{m}$  and 1.8  $\mu\text{m}$   
SN003-003-03624-2, PB2000-102878
- SP 250-54 Optical Fiber Power Meter Calibrations at NIST  
SN003-003-03652-8, PB2000-106986
- SP 250-56 Optical Fiber Power Meter Nonlinearity Calibrations at NIST  
SN003-003-03653-6, PB2000-106987
- SP 250-57 Measurement Assurance Program for the Spectral Density of Relative Intensity Noise of Optical Fiber Sources Near 1550 nm

\* Entries containing a stock number (SN003-003-) can be purchased from the Superintendent of Documents, U.S. Government Printing Office, Washington, DC 20402-9325. GPO will accept checks, money orders, VISA, and MasterCard. For more information, or to place an order, call (202) 512-1800. Be sure to cite the stock number on all orders.

Entries containing PB numbers can be purchased from the National Technical Information Service, Springfield, VA 22161. NTIS will accept American Express in addition to the payment methods listed for GPO. For more information or to place an order call (800) 553-6487. Fax: (703) 321-8547. Be sure to cite the PB number on all orders.

Entries without stock or PB numbers are in preparation.

# **NIST** *Technical Publications*

## **Periodical**

---

**Journal of Research of the National Institute of Standards and Technology**—Reports NIST research and development in those disciplines of the physical and engineering sciences in which the Institute is active. These include physics, chemistry, engineering, mathematics, and computer sciences. Papers cover a broad range of subjects, with major emphasis on measurement methodology and the basic technology underlying standardization. Also included from time to time are survey articles on topics closely related to the Institute's technical and scientific programs. Issued six times a year.

## **Nonperiodicals**

---

**Monographs**—Major contributions to the technical literature on various subjects related to the Institute's scientific and technical activities.

**Handbooks**—Recommended codes of engineering and industrial practice (including safety codes) developed in cooperation with interested industries, professional organizations, and regulatory bodies.

**Special Publications**—Include proceedings of conferences sponsored by NIST, NIST annual reports, and other special publications appropriate to this grouping such as wall charts, pocket cards, and bibliographies.

**National Standard Reference Data Series**—Provides quantitative data on the physical and chemical properties of materials, compiled from the world's literature and critically evaluated. Developed under a worldwide program coordinated by NIST under the authority of the National Standard Data Act (Public Law 90-396). NOTE: The Journal of Physical and Chemical Reference Data (JPCRD) is published bi-monthly for NIST by the American Chemical Society (ACS) and the American Institute of Physics (AIP). Subscriptions, reprints, and supplements are available from ACS, 1155 Sixteenth St., NW, Washington, DC 20056.

**Building Science Series**—Disseminates technical information developed at the Institute on building materials, components, systems, and whole structures. The series presents research results, test methods, and performance criteria related to the structural and environmental functions and the durability and safety characteristics of building elements and systems.

**Technical Notes**—Studies or reports which are complete in themselves but restrictive in their treatment of a subject. Analogous to monographs but not so comprehensive in scope or definitive in treatment of the subject area. Often serve as a vehicle for final reports of work performed at NIST under the sponsorship of other government agencies.

**Voluntary Product Standards**—Developed under procedures published by the Department of Commerce in Part 10, Title 15, of the Code of Federal Regulations. The standards establish nationally recognized requirements for products, and provide all concerned interests with a basis for common understanding of the characteristics of the products. NIST administers this program in support of the efforts of private-sector standardizing organizations.

*Order the following NIST publications—FIPS and NISTIRs—from the National Technical Information Service, Springfield, VA 22161.*

**Federal Information Processing Standards Publications (FIPS PUB)**—Publications in this series collectively constitute the Federal Information Processing Standards Register. The Register serves as the official source of information in the Federal Government regarding standards issued by NIST pursuant to the Federal Property and Administrative Services Act of 1949 as amended, Public Law 89-306 (79 Stat. 1127), and as implemented by Executive Order 11717 (38 FR 12315, dated May 11, 1973) and Part 6 of Title 15 CFR (Code of Federal Regulations).

**NIST Interagency Reports (NISTIR)**—A special series of interim or final reports on work performed by NIST for outside sponsors (both government and nongovernment). In general, initial distribution is handled by the sponsor; public distribution is by the National Technical Information Service, Springfield, VA 22161, in paper copy or microfiche form.

**U.S. Department of Commerce**  
National Institute of Standards  
and Technology  
325 Broadway  
Boulder, CO 80303-3328

Official Business  
Penalty for Private Use \$300

